

**University of Stuttgart**  
Germany

---

# Calculation of Alkaline-Earth Rydberg Atom Wavefunctions and Dipole Matrix Elements

---

BACHELOR THESIS

Submitted to the University of Stuttgart by  
Achim Nano Scholz

September 18, 2020

Examiner:  
Prof. Dr. Tilman Pfau

5. Physikalisches Institut  
Pfaffenwaldring 57, 70569 Stuttgart, Germany



## Abstract

Alkaline-earth atoms have lately gained in relevance as candidates for circular Rydberg atom preparation to be used in quantum simulators. In this thesis, the calculation of Rydberg electron wavefunctions and dipole matrix elements for  $^{88}\text{Sr}$  is discussed and implemented. Considerations about different approaches regarding atomic potentials and numerical methods are described by discussing limitations. As an powerful, yet simple approach a Coulomb approximation is pursued. To compensate for errors in this approach, quantum defects are gathered and arithmetically expanded for further usage. The obtained results for wavefunctions and dipole matrix elements are set in context with numerical methods implemented by other works.

## Zusammenfassung

Die Benutzung von Erdalkali Atomen als Basis für die Erzeugung zirkularer Rydberg Zustände, welche in Quantensimulatoren genutzt werden können, hat in den letzten Jahren deutlich an Relevanz gewonnen. In dieser Arbeit wird die Berechnung von Wellenfunktionen und Dipolmatrixelementen für  $^{88}\text{Sr}$  diskutiert und implementiert. Es werden verschiedene Lösungsverfahren, welche Atom-Potentiale und numerische Verfahren verwenden auf ihre Einschränkungen untersucht. Eine Coulomb Näherung wird als effizienter Ansatz eingeführt. Um mögliche Fehler der Näherung zu kompensieren, werden Quantendefekte gesammelt und für die weitere Nutzung rechnerisch erweitert. Die errechneten Wellenfunktionen und Dipolmatrixelemente werden mit anderen numerischen Methoden verglichen, um die Genauigkeit der Rechnung abschätzen zu können.

## **Ehrenwörtliche Erklärung**

Ich erkläre hiermit, dass ich die vorliegende Arbeit selbständig verfasst und nur unter Verwendung der angegebenen Quellen und Hilfsmittel angefertigt habe. Alle wörtlich und sinngemäß aus anderen Werken übernommene Aussagen sind als solche gekennzeichnet. Die vorliegende Arbeit war weder vollständig noch in Teilen Gegenstand eines anderen Prüfungsverfahrens. Weiterhin stimmt das elektronische Exemplar mit der gedruckten Version überein.

Stuttgart, den 18. September 2020

---

Achim Nano Scholz



# Contents

<b>1. Introduction</b>	<b>1</b>
<b>2. Theoretical Foundation</b>	<b>3</b>
2.1. Rydberg Atoms	3
2.2. Schrödinger Equation	4
2.2.1. Hydrogen	4
2.2.2. Divalent Atoms	5
2.2.3. Numerov Algorithm	6
2.3. Dipole Transitions	7
2.3.1. Dipole Approximation	7
2.3.2. Dipole Matrix Elements	7
2.3.3. Selection Rules	8
<b>3. Model Potential Approach</b>	<b>9</b>
3.1. Formulation of Atom Potentials	9
3.1.1. Screened Coulomb Potential	9
3.1.2. Polarization Potential	10
3.1.3. Fine Structure Term	11
3.1.4. Angular Momentum Terms	11
3.2. Discussion of the Approach	12
<b>4. The Quantum Defect</b>	<b>13</b>
4.1. Theoretical Introduction	13
4.1.1. Energy Shift	13
4.1.2. Physical Properties of the Quantum Defect	13
4.2. Determination of Strontium Quantum Defects	15
4.3. Error Compensation in the Coulomb Approximation	17
<b>5. Coulomb Approximation</b>	<b>19</b>
5.1. Idea of the Approximation	19
5.2. Python Implementation	22
5.2.1. Characterize Strontium States: <i>sr_state_properties.py</i>	22
5.2.2. Calculate Radial Wavefunctions: <i>sr_wavefunction.py</i>	22
5.2.3. Calculate Dipole Matrix Elements: <i>sr_dipolematrixelement.py</i>	25
5.2.4. Implementation Example	28
5.3. Limitations	30
5.3.1. Physical Limitations	30
5.3.2. Implementation Limitations	31
<b>6. Results and Discussion</b>	<b>37</b>
<b>7. Summary and Outlook</b>	<b>49</b>
<b>A. Appendix</b>	<b>51</b>
A.1. Quantum Defects of Strontium	51
<b>8. Bibliography</b>	<b>55</b>



# 1. Introduction

Ever since computational physics exists it is of interest to simulate physical systems. Starting from classical systems defined by classical differential equations, those methods also found their way into quantum systems. Here simulations now face the difficulty to process an “exploding amount of data”. This problem was outlined by R. P. Feynman [1] in 1981 who proposed a solution using quantum computers instead of classical computers which can simulate problems by using quantum systems themselves. Those simulation systems should be more accessible and better tuneable than the target systems. This proposal did become reality when in the last twenty years the first realizations of quantum simulators were achieved which are capable of simulating specific analogous systems [2].

Such quantum simulators have been implemented using numerous methods [3]. As in principle every well controllable quantum system is a candidate, multiple methods have been proven to be a good approach. The start was made in 1999 by nuclear magnetic resonance methods [4] used to simulate dynamics of quantum oscillators. Approximately ten years later, superconducting circuits [5], which promise a good individual control, were demonstrated. They were accompanied by trapped ions [6, 7] and ultracold quantum gases [8]. In the same time span an approach was introduced using photons [9], which was however not yet demonstrated experimentally at the time of this thesis. In the last years, two new systems were proposed. First to be mentioned is the usage of quantum dot arrays [10] in semiconductors. The second, very promising approach is the employment of neutral atoms trapped in optical tweezers.

In particular the use of highly excited Rydberg states proved very promising and comes with many advantages. Highly excited Rydberg states provide strong long-range interactions, which allows fast operation, while maintaining long coherence times. These effects are combined good laser accessible. Rydberg quantum simulators have been demonstrated recently with low- $L$  Rydberg states [11, 12, 13]. These implementations are however limited by the Rydberg state lifetime, which can be challenged by using circular Rydberg states. Circular Rydberg states come with high lifetimes thus impressive coherence times. This approach was proposed by the Haroche group [14] in a cryogenic environment and recently adapted by our group [15] to higher principle quantum numbers and room temperature environment. The setup of such a quantum simulator consists of single atoms trapped in an array of optical microtraps that provide an accessible system which can also be manipulated with ease. The individual trapping combined with the application of circular states allows for trapped Rydberg states which for low- $L$  states is only possible with more complex trap geometries, such as holocore beam traps [16].

Many trapped Rydberg atom experiments are realized using well known alkali atoms like rubidium [17]. This established method has lately been expanded to alkaline-earth atoms which promise advantages over one-electron systems [18]. Alkaline-earth atoms are well suited for laser cooling using weak intercombination lines and magic wavelength optical trapping [19]. The absence of a nuclear spin and the second valence electron, which can be used for fluorescence imaging without disturbing the Rydberg state, renders strontium  $^{88}\text{Sr}$  as a promising candidate. Further, strontium has a level scheme offering two clock transitions from the ground state  $5s5s\ ^1S_0$  to the  $5s5p\ ^3P_0$  [20] and  $5s5p\ ^3P_1$  [21] states and generally well accessible laser-wavelengths. Due to these promising properties,  $^{88}\text{Sr}$  is already used in numerous ultracold atom experiments [22, 23, 24].

The use of circular Rydberg states also brings new challenges concerning their creation and detection compared to low- $L$  Rydberg states. Since many quanta of angular momentum have to be transferred, direct laser excitation is hardly possible, but adiabatic transfer schemes must be used [25, 26]. Those states rely heavily on the coupling between different Rydberg state manifolds. Further, the use of Rydberg states as qubit states requires exact knowledge of the coupling to surrounding states. Therefore it is necessary to calculate the wavefunctions and dipole transitions of strontium Rydberg states to a high precision. Up to this point, there is not much theoretical work available for  $^{88}\text{Sr}$ . In the scope of this thesis a one-electron treatment of the complex divalent atom strontium is introduced to allow numerical calculations of wavefunctions and thus dipole matrix elements of  $^{88}\text{Sr}$  using collected quantum defect data. Different readily available methods and implementations are included for comparison. The results of this work provide a versatile basis for further calculation of Stark maps and Zeeman shifts in strontium.

## Outline

In the first chapter, theoretical foundations for the further discussions and implementations are given. To discuss possible approximations a method using atomic model potentials is introduced and outlined in chapter 3. This chapter also gives a detailed introduction to atomic potentials of alkaline-earth atoms.

This is followed by chapter 4 where the importance of quantum defects in alkaline-earth atoms is described and underlined. Furthermore, a database for strontium quantum defects is calculated using a fitting procedure on experimental values. The calculated data is used in chapter 5 where a Coulomb approximation of the Schrödinger equation is proposed, implemented and discussed. The implementation is done in form of python classes which is also documented in detail. Potential errors and limitations of the approach are considered to outline possible results. The obtained wavefunctions and dipole matrix elements are put into context in chapter 6 by comparing to other methods. For this purpose a wavefunction and dipole matrix element implementation by Weber et al. [27] is used besides the alkali Rydberg calculator [28], which only implements dipole matrix elements.

At the end of the work a summary of the current status is given. Furthermore, future implementations and general goals of the calculation procedure are outlined.

## 2. Theoretical Foundation

In this chapter, an overview of the theoretical foundation needed in the course of this work will be given, starting with the basic properties of Rydberg atoms. An overview of the Schrödinger equation and its solution follows with the main focus on the so-called Numerov method. Finally a brief introduction of dipole transitions moments, which are the main interest of this work, will be given.

### 2.1. Rydberg Atoms

Rydberg atoms are characterized by their highly excited valence electron. Many atom properties scale with the excitation to high principal quantum numbers  $n$ , which leads to interesting effects in Rydberg states. The theory behind Rydberg atoms is discussed very detailed in T. F. Gallagher's "Rydberg Atoms" [29]. Here the most important information about Rydberg atoms in the frame of this work should be given.

#### Property Scaling

The Rydberg states are often described with the semi-classical Bohr theory, as the excited electron reaches large orbits. The formula for energies of the Rydberg states is in the semi-classical case given by

$$E = -\frac{R}{n^2} \quad (2.1)$$

where  $R$  denotes the Rydberg constant which is an experimentally determined property of the atom. The atomic potential, seen by electrons in Rydberg states, furthermore approaches the Coulomb case, as will be discussed in later chapters.

With decreasing eigenenergies the wavefunction and therefore the orbit radius of the electron increase in size. The energies scale with  $n^{-2}$  which leads to a scaling of the orbit radius with  $n^2$ . The low binding energies of Rydberg states is also the main limitation for the size, as small field fluctuations can easily disturb the electron wavefunction and even ionize highly excited Rydberg atoms.

The scaling of the principal quantum number also effects the electron transitions: The radiative lifetime scales with  $n^3$  and the dipole moment scales with  $n^2$ . As these properties can also be observed in later calculations, it is necessary to keep the scaling in mind.

As the scaling of all properties is always given with the principal quantum number, it seems necessary to discuss, what high principal quantum numbers are. This is not specified in any literature but it seems reasonable to choose  $n = 20$  as the lowest  $n$  for Rydberg states in the context of this work.

#### Circular Rydberg States

In the introduction, so-called circular Rydberg states were mentioned as Rydberg states with extremely long coherence times. Physically, circular states are just states with the

maximal possible angular momentum quantum number  $L = n - 1$ . This leads to large orbit radii, which is why circular states can be treated nearly classical. Circular Rydberg states possess many more interesting properties which are beyond the scope of this work but can be found in literature [30].

### Rydberg Wavefunctions

Since the goal of this work is to obtain dipole matrix elements from Rydberg wavefunctions of strontium, it is important to mention how these wavefunctions behave. In figure 2.1 the radial wavefunction, in form of a probability density, of the  $5s50s^1S_0$  state in  $^{88}\text{Sr}$  can be seen as a plot over the radius  $r$ .

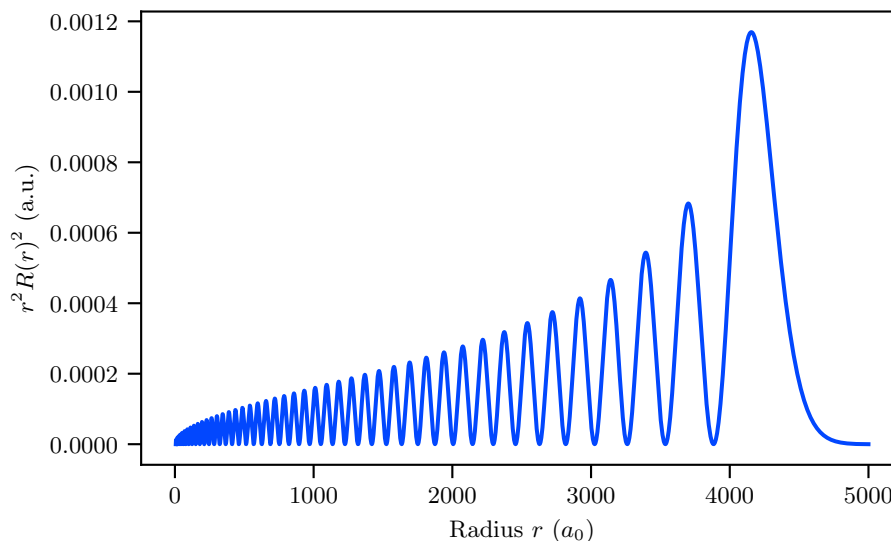


Figure 2.1.: Calculated radial wavefunction of the  $5s50s^1S_0$  state in  $^{88}\text{Sr}$ . For better visualization the plot shows the radial probability density  $r^2 R(r)^2$  where  $R(r)$  denotes the radial wavefunction.

Typical for Rydberg wavefunctions are the oscillating amplitudes which reach their maximum at the outermost peak before decaying to zero. The radius value of the outer maxima corresponds to the orbit radius  $\langle r \rangle$ .

## 2.2. Schrödinger Equation

The Schrödinger equation describes the motion of the electron in the atomic potential and gives the frame for wavefunction calculation. In this section a theoretical introduction of the basic equation should be given which will be needed later on.

### 2.2.1. Hydrogen

The quantum mechanical treatment of hydrogen via the Schrödinger equation is of significant historical interest as it is known since 1926. Considerations about the solution can be used also to approximate other atoms and to understand Schrödinger equations of higher complexity. The generic form of the Schrödinger equation is given by

$$\left[ -\frac{\nabla^2}{2} + V(r) \right] \psi = E\psi \quad (2.2)$$

where  $E$  denotes the eigenenergy and  $V(r)$  is the atomic potential classically given as  $V(r) = r^{-1}$ . The function  $\psi$  denotes the total wavefunction. As the problem is radially symmetric, the equation is typically described in spherical coordinates, where the wavefunction  $\psi$  depends on  $r$ ,  $\theta$  and  $\varphi$ . It is convenient to separate via

$$\psi(r, \theta, \varphi) = R(r)Y(\theta, \varphi) \quad (2.3)$$

where  $R(r)$  denotes the radial wavefunction and  $Y(\theta, \varphi)$  denotes the angular wavefunction. The further calculation of both solutions is done in great detail by many authors. A good overview can be found in [31, pp. 22-29] where the solution of the angular wavefunction is given by

$$Y_{l, m_l} \propto (l_-)^{l-m_l} \sin^l \theta \exp(il\varphi). \quad (2.4)$$

Here  $l_-$  denotes the lowering operator of the angular momentum quantum number. The angular wavefunction only defines the spatial shape of the total wavefunction and is often of reduced interest when calculating atomic properties. More important is the radial wavefunction which is obtained by solving the radially dependent part of the Schrödinger equation. This is done by introducing  $u(r) = rR(r)$  for which now the equation simplifies to

$$\left[ -\frac{d^2}{dr^2} + \frac{l(l+1)}{r^2} - \frac{1}{r} \right] u(r) = Eu(r). \quad (2.5)$$

This differential equation is commonly known as the Coulomb equation which can be solved via the Numerov method introduced in section 2.2.3.

### 2.2.2. Divalent Atoms

The hydrogen atom discussed above outlines the general idea of solving the Schrödinger equation. This will also help to study divalent atoms which are much more complicated, since new effects arise induced by the interaction between the two valence electrons.

As the complicated calculations with divalent atoms in general are beyond the scope of this work, only some brief discussion on the theory will be done. A detailed discussion on this topic is provided by Bransden et al. [32]. The Schrödinger equations of two electron systems is given by

$$\left[ -\frac{\nabla_{\mathbf{r}_1}^2}{2} - \frac{\nabla_{\mathbf{r}_2}^2}{2} - \frac{Z}{r_1} - \frac{Z}{r_2} + \frac{1}{r_{12}} \right] \psi(\mathbf{r}_1, \mathbf{r}_2) = E\psi(\mathbf{r}_1, \mathbf{r}_2) \quad (2.6)$$

where valence electron interactions are included via the  $r_{12}^{-1}$  term.

### Symmetry of the Wavefunctions

Wavefunctions of divalent atoms are coupled due to the fact that interaction terms of both electrons make them inseparable. This means especially that the wavefunction solutions can not be expressed as simple products of single-particle wavefunctions. Interesting to discuss are symmetries of the entangled solutions. Therefore an interchange operator  $P_{12}$  is introduced that permutes the two valence electrons. The wavefunctions

$$\psi(\mathbf{r}_2, \mathbf{r}_1) = P_{12}\psi(\mathbf{r}_1, \mathbf{r}_2) \quad (2.7)$$

and  $\psi(\mathbf{r}_1, \mathbf{r}_2)$  satisfy the same Schrödinger equation which leads to the relation

$$\psi(\mathbf{r}_2, \mathbf{r}_1) = \pm\psi(\mathbf{r}_1, \mathbf{r}_2). \quad (2.8)$$

This defines now if solutions of the Schrödinger equation are symmetric (+) or antisymmetric (-) wavefunctions. Those two cases correspond to the singlet- and triplet-states, where singlet-states correspond to symmetric wavefunctions  $\psi_+$  and triplet-states correspond to antisymmetric wavefunctions  $\psi_-$ . In later chapters these two valence shell configurations will be treated as two independent series which are separated only by their energy.

### Solution Methods

A common approximation for solving equation (2.6) is to neglect the interaction term  $r_{12}^{-1}$ . This approximation is called individual particle approximation and makes it possible to propose a separation ansatz

$$\psi = \psi(1)\psi(2) \quad (2.9)$$

which leads to separate equations for both electrons. These equations can now be solved individually like one-electron systems. This approximation could be made in general to any multi-electron system but neglecting interaction forces can lead to significant errors for low  $n$  states where the typical electron separation is small.

Besides the individual particle approximation it is also possible to solve the problem with included interactions. This comes with many mathematical complications and makes it necessary to introduce complex solving methods like the so-called multi-configuration Hartree-Fock theory. These methods are discussed by C. Froese Fischer [33] and Vaeck et al. [34] but will not be further used in the scope of this work.

#### 2.2.3. Numerov Algorithm

Since the Schrödinger equation is just analytically solvable for a few special cases, it is necessary to introduce numerical solution methods. The Numerov algorithm is the most common method when calculating simple, one-dimensional differential equations as for example the Schrödinger equation of hydrogen. It was first introduced by B. V. Numerov (see also Nomerov) [35] and is described in many newer publications.

The algorithm is capable of solving all differential equations of the form

$$\frac{d^2 f(x)}{dx^2} = -g(x)f(x) + s(x) \quad (2.10)$$

by discretizing the domain of  $f(x) \rightarrow f_n$  in equally distant steps  $\delta x$  where  $n$  denotes the step-number. This yields the iterative relation

$$\begin{aligned} f_{n+1} \left( 1 + \frac{(\delta x)^2}{12} g_{n+1} \right) = & 2f_n \left( 1 - \frac{5(\delta x)^2}{12} g_n \right) - f_{n-1} \left( 1 + \frac{(\delta x)^2}{12} g_{n-1} \right) \\ & + \frac{(\delta x)^2}{12} (s_{n+1} + 10s_n + s_{n-1}) \end{aligned} \quad (2.11)$$

where terms of  $\mathcal{O}((\delta x)^6)$  are neglected. This relation allows to obtain an out- or inward integration by rearranging the equation either for  $f_{n+1}$  or  $f_{n-1}$ .

As the method will be used later to calculate Rydberg wavefunctions, it is useful to describe the implemented algorithm. The equation which has to be solved is of the form of equation (2.5). The problem will be solved as an inward integration. The term  $s(x)$  mentioned in equation (2.11) is zero for the Schrödinger equation so the steps of the function

$u(r)$  are given by

$$u_{n-1} = \frac{2u_n \left(1 - \frac{5(\delta r)^2}{12} g_n\right) - u_{n+1} \left(1 + \frac{(\delta r)^2}{12} g_{n-1}\right)}{\left(1 + \frac{(\delta r)^2}{12} g_{n-1}\right)} \quad (2.12)$$

where  $g(r)$  is given by

$$g(r) = V(r) + E. \quad (2.13)$$

The solution of equation (2.5) is obtained by calculating a defined range step-wise from given initial values at the outermost point of  $u(r)$ .

## 2.3. Dipole Transitions

Between two electronic states, characterized by their quantum numbers and the eigenenergy, electromagnetic transitions of different order are possible. This section will give a short introduction to electric dipole transitions and their quantum mechanical treatment.

### 2.3.1. Dipole Approximation

Optical transitions in general are treated as an interaction of an electric light field with the atom. The electric moments of this field can be expanded in a multipole expansion [36] where all multipole terms are neglected except the dipole moment term. This is called “dipole approximation” and introduces a perturbation ansatz

$$H = H_0 - \mathbf{d} \cdot \mathbf{E} \quad (2.14)$$

where  $\mathbf{d}$  denotes the transition dipole moment defined as

$$\mathbf{d} = -e\mathbf{r}. \quad (2.15)$$

This ansatz can now be used to derive properties of dipole transitions.

### 2.3.2. Dipole Matrix Elements

Transitions between atomic states, and therefore the dipole transition moments, depend on the wavefunctions of the states and their overlap. The property describing this transition is called dipole matrix element and is defined as

$$\begin{aligned} \langle 1|\mathbf{r}|2\rangle &= \int_0^\infty R_{n_1, L_1}(r) r R_{n_2, L_2}(r) r^2 dr \int_0^{2\pi} \int_0^\pi Y_{n_1, L_1}^*(\theta, \varphi) \frac{\mathbf{r}}{r} Y_{n_2, L_2}^*(\theta, \varphi) \sin \theta d\theta d\varphi \\ &= \mathcal{R}_{12} \mathcal{I}_{\text{angular}} \end{aligned} \quad (2.16)$$

for transitions from state 1 to state 2 [31]. Here  $R(r)$  and  $Y(\theta, \varphi)$  denote the radial and the angular part of the electron wavefunction. Dipole matrix elements are used to calculate properties of the transitions like lifetimes and transition probabilities. Furthermore the angular part of the dipole matrix element includes the well-known selection rules and can also be written by using Wigner symbols. This leads to a property called reduced dipole matrix element which is defined as

$$\langle L_1|r|L_2\rangle = (-1)^{L_1} \sqrt{(2L_1 + 1)(2L_2 + 1)} \underbrace{\begin{pmatrix} L_1 & 1 & L_2 \\ 0 & 0 & 0 \end{pmatrix}}_* \mathcal{R}_{n_1 L_1, n_2 L_2} \quad (2.17)$$

where  $*$  is a Wigner-3j symbol. The Wigner symbols, introduced by E. P. Wigner [37], implement Clebsch-Gordan-Coefficients and selection rules for transitions. This representation of the reduced dipole matrix element makes it possible to calculate dipole matrix elements solely from radial dipole matrix elements and the angular quantum numbers.

The previous calculation just allows transitions between  $L$  degenerate states and does not include fine structure. This can be changed by coupling the angular momentum quantum number and the spin to the total angular momentum  $J$  via

$$\langle J_1|r|J_2\rangle = (-1)^{L_1+s+J_2+1}\sqrt{(2J_1+1)(2J_2+1)}\underbrace{\begin{bmatrix} J_1 & 1 & J_2 \\ L_2 & S & L_1 \end{bmatrix}}_{**}\langle L_1|r|L_2\rangle \quad (2.18)$$

where  $**$  is a Wigner-6j symbol. Furthermore the Wigner-Eckart theorem

$$\langle n, J_1, m_{J_1}|r|n, J_2, m_{J_2}\rangle = (-1)^{J_1-m_{J_1}}\begin{pmatrix} J_1 & 1 & J_2 \\ -m_{J_1} & -q & m_{J_2} \end{pmatrix}\langle J_1|r|J_2\rangle \quad (2.19)$$

can be used to write a resulting dipole matrix element dependent on the projection of the total angular momentum of both states [38].

### 2.3.3. Selection Rules

The selection rules for dipole transitions, mentioned in section 2.3.2, are obtained by the integral over the angular wavefunctions in equation (2.16). This integral vanishes for certain constellations of the quantum numbers which leads to so-called forbidden transitions where respectively the whole dipole matrix vanishes. In addition to these selection rules, the parity of the wavefunctions also introduces further restrictions. The complete theory behind the selection rules is described in detail in [39]. Here, just a short overview should be given to also understand, what the Wigner symbols implement. All rules are denoted in the notation of multivalent atoms but also apply to one-electron atoms.

The spin quantum number  $S$  is subject to the selection rule  $\Delta S = 0$  in the case of a small spin-orbit coupling. As alkaline-earth atoms are heavy atoms and therefore have a large spin-orbit coupling, this selection rule is not valid at least for the ground states. For Rydberg states it is assumed that the selection rule is valid to appoint to separate the singlet and triplet series.

For the angular momentum quantum number  $L$  the rule  $\Delta L = \pm 1$  generally applies. When  $\Delta S = 0$  applies the selection rule for  $L$  can be expanded to  $\Delta L = 0, \pm 1$ .

The total angular momentum quantum number selection rules are  $\Delta J = 0, \pm 1$  where  $J_1 = 0 \rightarrow J_2 = 0$  is forbidden. The change of the magnetic quantum number furthermore describes the polarization of the transition. Here, the selection rule  $\Delta m_J = 0$  implies a linear polarized transition, ergo  $\pi$ -light. For  $\Delta m_J = \pm 1$  the transition is circular polarized where  $+1$  denotes  $\sigma^+$ -light and  $-1$  denotes  $\sigma^-$ -light.

All selection rules are introduced in further calculations via the Wigner symbols already mentioned above. Since it is not possible to evaluate the symbols without further knowledge of the formalism, it is useful to keep the selection rules in mind.

## 3. Model Potential Approach

The model potential approach describes the method of using model potentials to approximate atomic potentials for valence electrons. It is commonly used for alkali atoms where multiple model potentials are defined which can be fitted on experimental data for high accuracy approximations. This chapter will focus on model potentials for alkaline-earth atoms and their issues in terms of solving the Schrödinger equation.

### 3.1. Formulation of Atom Potentials

Atom potentials combine different effects which influence the eigenstates of the atoms, namely the electron states. This section should give a detailed overview over potential terms and their physical background. Furthermore different forms of alkaline-earth potentials are discussed.

#### 3.1.1. Screened Coulomb Potential

The Coulomb term in potentials generally describes the electrostatic interaction between the core and the electrons. In the most simple case, namely the hydrogen atom, the term simplifies to

$$V_C(r) = -\frac{1}{r} \quad (3.1)$$

where  $r$  denotes the radial coordinate of the radially symmetric problem. The potential is purely attractive.

For more complicated one-electron systems like alkali atoms this potential needs to be modified, since the core potential is partially screened by the electrons of the closed electron-shells. This effect is treated by using the so-called central-field approximation which summarizes the closed-shell electrons in one electric field which can be integrated into a modified Coulomb potential. A detailed discussion of this process is given by C. J. Foot [31, pp. 64-68].

As for the described approach only the form of the potential is interesting, a derivation by the means of the frame conditions described in [38, pp. 179-180] as

$$V_S(r) = \begin{cases} -\frac{Z}{r} & r \rightarrow 0 \\ -\frac{1}{r} + V_{C,\text{mod}}(r) & \text{in between} \\ -\frac{1}{r} & r \rightarrow \infty \end{cases} \quad (3.2)$$

where  $Z$  denotes the nuclear charge, is satisfactory. For the modified Coulomb potential the simple example

$$V_{C,\text{mod}}(r) = \frac{-(Z-1)e^{-\frac{r}{r_S}}}{r} \quad (3.3)$$

can be chosen, where  $r_S$  is a variable screening radius. In equation (5.11) an actual screened Coulomb potential for Rb<sup>87</sup> is used. This potential was introduced by Marinescu et al. [40]

and includes more pre-factors for the exponential term. This principle can often be found in alkali model potentials and is used to fit model potentials on experimental values. By determining fitting parameters one can now do wavefunction calculations which is also the basic principle behind the model potential approach in general.

In divalent atoms, like the alkaline-earth atoms, it is necessary to treat the electrostatic interaction of both electrons with the core and between each other. The most simple example would be the helium case. This system includes a potential energy of

$$E_{\text{pot}} = - \left( \frac{Z}{r_1} + \frac{Z}{r_2} - \frac{1}{r_{12}} \right) \quad (3.4)$$

where  $r_i$  ( $i = 1, 2$ ) denotes the distance of the electrons to the core and  $r_{12}$  denotes the distance between the electrons. However this problem is hard to calculate and not practicable for implementations. To solve the problem the divalent system is separated into two one-electron systems which, in the most simple case, do not interact with each other. This approximation now leads back to the alkali case, but now with two terms for two electrons which are both interacting with a screened core. The screened Coulomb term therefore is simply given by

$$V_S(r) = -\frac{1}{r} \left[ 2 + (Z - 2) e^{-a_1(L)r} + a_2(L)r e^{-a_3(L)r} \right] \quad (3.5)$$

with fitting parameters  $a_i(L)$  ( $i = 1, 2, 3$ ), which is the same potential as in equation (5.11) but modified for strontium in this case [41, p. 18]. This screened Coulomb potential now describes a single ionized strontium atom. To still get both electrons into the picture it is necessary to sum up equation (3.5) two times and replace  $r$  with  $r_i$  ( $i = 1, 2$ ) to get a total Coulomb potential

$$V_C(r_1, r_2) = \sum_{i=1}^2 V_C(r_i). \quad (3.6)$$

One has to be careful, since interaction processes are neglected. A simpler form of this potential can be seen in [42] where an unscreened Coulomb potential is used.

#### 3.1.2. Polarization Potential

Atomic potentials are not only depending on direct electrostatic interactions but also on the dynamic core polarization by the order of  $r^{-4}$ . This effect occurs because the valence electrons interact with the so-called ionic core, consisting of the nucleus and the closed electron-shells. The interaction with the core can be understood as a change in the charge distribution induced by the valence electron. This change depends on the core polarizability  $\alpha_c$  which is an experimental or simulated fixed value.

The treatment of polarization terms is important because it reduces errors which result from the frozen-core approximation [42]. This approximation describes the treatment of the core as a fixed charge distribution with the nuclear charge  $Z$ .

The detailed calculation of the polarization potentials is beyond the scope of this work and is treated in detail in [42] and [43]. The conclusion of both papers is a potential

$$V_{\text{pol}}(r_1, r_2) = -\frac{\alpha_c}{2r_1^4} w^2(r_1) - \frac{\alpha_c}{2r_2^4} w^2(r_2) - \alpha_c \frac{r_1 \mathbf{e}_{r_1} \cdot r_2 \mathbf{e}_{r_2}}{r_1^3 r_2^3} w(r_1) w(r_2) \quad (3.7)$$

which includes the core polarisability and two cutoff functions  $w(r)$ . This potential treats both effects of single valence electrons and also interaction effects between both valence electrons.

To give another example for polarization potentials, the more simple formulation of R. Mukherjee [41]

$$V_{\text{pol}}(r) = \frac{\alpha_c}{2r^4} \left[ 1 - e^{-\left(\frac{r}{r_L}\right)^6} \right] \quad (3.8)$$

for a single electron system can be mentioned. This approach does not treat interactive processes of both valence electrons.

Both potential term approaches are mostly interesting in low  $r$  and therefore low  $n$  regimes. Since this regime is not relevant when calculating Rydberg states, it would be unnecessary to include those terms. A detailed discussion on this topic is given in section 4.3 where an alternative to the polarization potential solution is given.

### 3.1.3. Fine Structure Term

Another term in the model potential approach is defined by the treatment of fine structure effects. Following [41] one can use the potential term

$$V_{\text{s.o.}}(r) = \frac{1}{4m^2c^2} \frac{1}{r} \frac{dV_S}{dr} [J(J+1) - L(L+1) - S(S+1)] \quad (3.9)$$

where  $V_C(r)$  is the Coulomb term defined in equation (3.5). As this term scales as  $r^{-1}$  and  $n^{-3}$  it can be neglected for Rydberg atoms but should be used for the calculation of ground states for example. It must be kept in mind that this term just denotes the potential induced by spin-orbit interaction and not the fine structure itself, which is important in all  $n$  regimes.

### 3.1.4. Angular Momentum Terms

Literature on atomic physics is inconsistent regarding the treatment of angular momentum terms in atomic potentials. Sometimes typical rotational barriers are used to model the shielding of the ionic core and sometimes  $L$ -dependent terms are included directly in the potentials. The most famous term regarding angular momentum influences is the so-called ‘‘centrifugal barrier’’

$$V_{\text{cb}}(r) = \frac{L(L+1)}{r^2} \quad (3.10)$$

which arises from the separation of the Schrödinger equation into a radial and angular part. Following [32] the Hamiltonian of the one dimensional Schrödinger equation in the one-electron system case can be written as

$$H = -\frac{\nabla^2}{2} + V(r) = -\frac{1}{2} \left[ \frac{1}{r^2} \partial_r (r^2 \partial_r) + \frac{1}{r^2 \sin \theta} \partial_\theta (\sin \theta \partial_\theta) + \frac{1}{r^2 \sin^2 \theta} \partial_\varphi^2 \right] + V(r) \quad (3.11)$$

where the Laplace operator in spherical coordinates can also be written as

$$\frac{1}{r^2} \partial_r (r^2 \partial_r) + \frac{1}{r^2 \sin \theta} \partial_\theta (\sin \theta \partial_\theta) + \frac{1}{r^2 \sin^2 \theta} \partial_\varphi^2 = \frac{1}{r^2} \partial_r (r^2 \partial_r) - \frac{\mathbf{L}^2}{r^2}.$$

By inserting into the Schrödinger equation and separating  $\psi(r, \theta, \varphi) = R(r)Y(\theta, \varphi)$

$$-\frac{1}{2} \left[ \frac{1}{r^2} \partial_r (r^2 \partial_r) - \frac{\mathbf{L}^2}{r^2} \right] R(r) + V(r)R(r) = ER(r) \quad (3.12)$$

is obtained which can be separated in the later used Coulomb equation (5.2). The centrifugal barrier is often used to define the effective potential

$$V_{\text{eff}}(r) = V(r) + \frac{L(L+1)}{2r^2}. \quad (3.13)$$

which is normally plotted when discussing potentials.

In the case of alkaline-earth atoms it is necessary to include effects of the second electron on angular momentum terms. Those effects are mostly interesting if the valence electrons have the same  $L$  and are both in a region near the ionic core. This case is included in the potential proposed by Fuentealba et al. [42]. For Rydberg states effects besides the centrifugal barrier should be negligible and therefore need not be treated in a potential approach.

## 3.2. Discussion of the Approach

In the last section two different examples of alkaline-earth model potentials were proposed. To implement the model potential, it is necessary to first fit the potentials to known experimental data. The conventional approach is to use energy data from spectroscopy experiments. The so obtained well defined potentials are then plugged into the Schrödinger equation which is discussed in detail in section 2.2.2. It is now necessary to solve the problem which will then return wavefunctions by minimizing the eigenenergies. As already mentioned in the discussion of the multivalent Schrödinger equation, this solving procedure is numerically difficult and inefficient when treating large  $n$  ranges.

At this point it is necessary to recap for what purpose an accurate atomic potential would be needed and if the complex calculation process is necessary to implement. As mentioned above the introduced potential terms, except the Coulomb term, are mostly significant for the calculation of low lying states and electron series where interaction effects are significantly large. For high  $n$  states, namely Rydberg states, most of the effects vanish due to low contributions. Since it is the goal of this work to calculate Rydberg atom wavefunctions and dipole matrix elements it appears to be reasonable to choose a simpler approach to the problem. This new approach must include a simple version of the atomic potential and other inputs of experimental values to compensate errors which result from the potential approximation.

One can now look again at the Schrödinger equation and check possible inputs. It is obvious that other approaches must contain some sort of variable modification which can for example be realized via the eigenenergies of the problem. This will be discussed in the next chapter 4 by introducing the quantum defect. The ansatz to choose simpler atomic potentials which will solve the problem of including electron-electron interactions is furthermore discussed in chapter 5.

## 4. The Quantum Defect

As discussed in section 3.2, a further approximation would need an input of experimental data in the wavefunction, which can be achieved via eigenenergies. This chapter will treat the theory behind the so-called quantum defects and explains their importance for the implementation of eigenenergies in the later used Coulomb approximation.

### 4.1. Theoretical Introduction

#### 4.1.1. Energy Shift

The idea of the quantum defect arises when observing Rydberg states and measuring their energies as shown in figure 4.1. It can be observed that the states seem to be shifted by a dynamic factor in relation to the respective hydrogen state. This observation can be explained by the already discussed effect that Rydberg states are mostly described by Coulomb like potentials. In hydrogen, where no other electrons occur, the potential is solely  $-r^{-1}$  wherever in more complex atoms the potential is disturbed by the shell electrons. The dynamic factor, which describes this disturbance and shifts the state energies, is known today as the quantum defect  $\delta$ . Its relation to the energy is given by the Rydberg formula (2.1) when introducing the effective principal quantum number  $n_{\text{eff}} = n - \delta$  as the shifted principal quantum number. The shifted energy in Hartree atomic units is then given by

$$E^{\text{a.u.}} = -\frac{hcR}{(n - \delta)^2} \quad (4.1)$$

where  $h$  denotes the Planck constant,  $c$  the speed of light in vacuum and  $R$  the Rydberg constant. This simple relation allows calculations of one property from the other, simply by knowing the principal quantum number of the state. As one wants to calculate exact eigenenergies as an input for the Schrödinger equation, it is necessary to have a database with exact quantum defects. This problem will later be discussed for strontium.

#### 4.1.2. Physical Properties of the Quantum Defect

The quantum defect is a versatile property which describes real physical effects. To understand the physical nature of the quantum defect one has to look again at the energy level scheme in figure 4.1. It can be seen that the quantum defect varies with different angular momentum quantum numbers. For increasing  $L$  the quantum defect vanishes. This behavior can be intuitively understood by considering the following analogy: The excited valence electron experiences a Coulomb potential at large distances which changes with decreasing distance. At some point the electron scatters at the shell consisting of the inner electrons [44]. As in scattering problems a phase shift occurs which is for example used in multichannel quantum defect theory. The phase shift like the energy shift itself, decreases for higher  $L$  since the centrifugal barrier increases. This can be thought of as an orbit which gets “rounder” and therefor the electron has a smaller probability density at the core. The effect will later on be discussed to possibly correct errors of the Coulomb approximation.

Additionally to this dependency on the angular momentum quantum number, the quantum

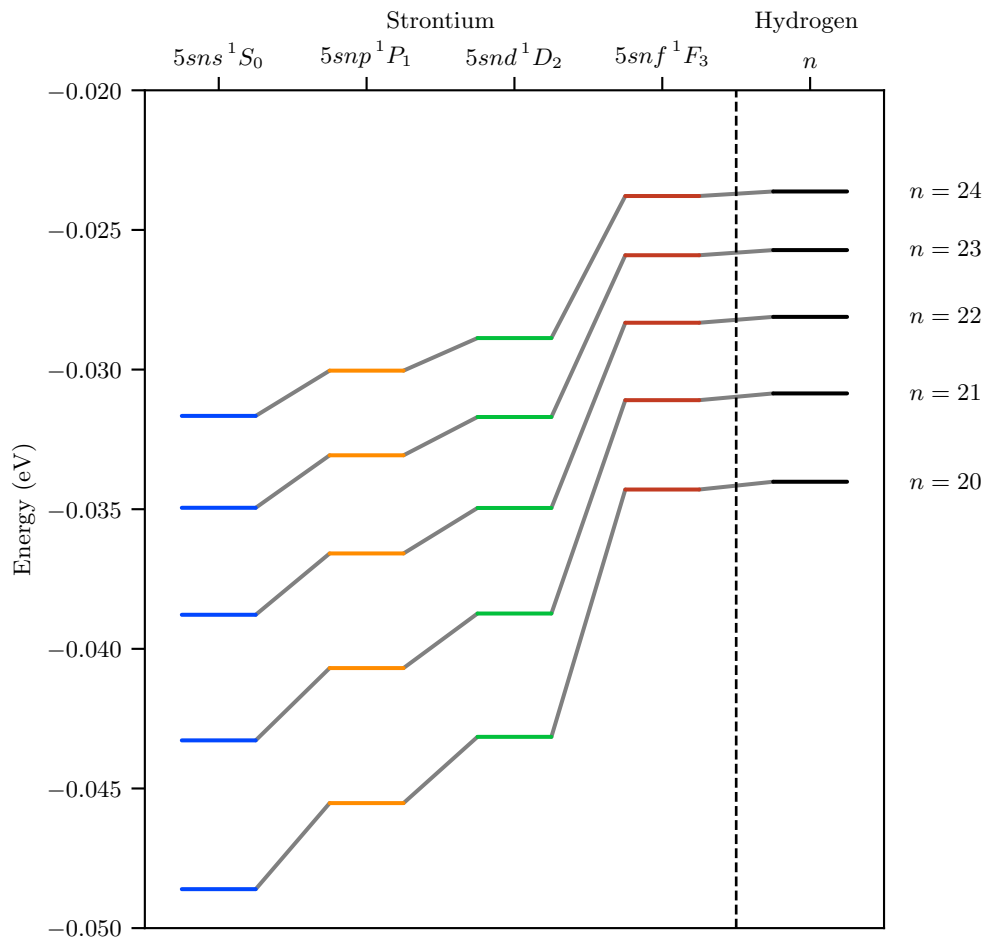


Figure 4.1.: Energies of the hydrogen and strontium singlet series states for  $20 \leq n \leq 24$  to show the energy shift described by the quantum defect. States with the same  $n$  are connected so one can observe the dependence of the quantum defect on the angular momentum quantum number  $L$ . It can be seen that for  $L \rightarrow 3$  the energy shift and therefore also the quantum defect nearly vanishes.

defects in alkaline-earths are also highly depending on the principal quantum number. This behavior is due to the existence of the second valence electron which is influencing the potential experienced by the excited electron. For principal quantum numbers in the region of the non-excited electron, the quantum defects show a resonance. That can be seen later and causes problems when calculating values in this region. For higher principal quantum numbers the electrons depart from each other and this effect vanishes. The quantum defects converge and can therefore be approximated quite good as discussed below.

An intersection between the physical and mathematical properties is the so-called Rydberg-Ritz formula

$$\delta = \delta_0 + \frac{\delta_2}{(n - \delta_0)^2} + \frac{\delta_4}{(n - \delta_0)^4} + \mathcal{O}(\delta_0^6) \quad (4.2)$$

which introduces a series expansion for the quantum defect with the Rydberg-Ritz-Coefficients  $\delta_i$  ( $i = 0, 2, 4$ ). This formula furthermore describes the quantum defect for a perturbation theory approach when disturbing the Coulomb potential hamiltonian with a short-range spherically symmetric correction potential as mentioned by Drake et al. [45]. The coefficients then have a physical significance as they can be associated with the  $c_i$  coefficients in

the potential formulation

$$V(r) = -\frac{1}{2} \left[ \frac{c_4}{r^4} + \frac{c_6}{r^6} + \mathcal{O}(r^{-7}) \right] \quad (4.3)$$

where  $c_4$  denotes the dipole polarizability and  $c_6$  denotes the corrected quadrupole polarizability. Including the  $\delta_2$  and  $\delta_4$  terms in equation (4.2) directly correlates with doing approximations under respect of the multipole polarizability.

## 4.2. Determination of Strontium Quantum Defects

As mentioned before it is necessary to determine the quantum defects up to a sufficient accuracy. For alkali elements like rubidium the quantum defect is dominated by an angular momentum quantum number  $L$  dependent  $\delta_0$  which has almost no  $n$  dependence. Therefore it is possible to just mention one quantum defect for each  $l$ -state. Those precise values were often measured and are therefore widely available. As an example for experimental data of rubidium quantum defects [46] can be mentioned.

As described above for alkaline-earths like strontium an  $n$ -dependency occurs which makes

Table 4.1.: List of quantum defects obtained by fitting equation (4.2) to the data listed in Appendix A.1. For every state the  $n$ -range is given since the fit does not converge for all  $n$  values. Fit functions and data are plotted in figure 4.2. The fitting parameters are rounded up to the numerical error given by the fit.

	State	Fit Range	$\delta_0$	$\delta_2$	$\delta_4$
$L = 0$	$5sns^1S_0$	$10 \leq n \leq 80$	3.268 942 7(7)	-0.1333(9)	0.7(1)
	$5sns^3S_1$	$11 \leq n \leq 45$	3.366(3)	2(1)	$-7(9) \times 10^1$
$L = 1$	$5snp^1P_1$	$10 \leq n \leq 29$	2.726(3)	-4(2)	$-1(2) \times 10^2$
	$5snp^3P_2$	$5 \leq n \leq 60$	2.882(2)	0.1(2)	4.5(9)
	$5snp^3P_1$	$5 \leq n \leq 22$	2.881(3)	0.5(1)	3.0(7)
	$5snp^3P_0$	$5 \leq n \leq 15$	2.883(6)	0.5(2)	2.9(9)
$L = 2$	$5snd^1D_2$	$15 \leq n \leq 80$	2.387 83(5)	$-4.548(9) \times 10^1$	$1.4(3) \times 10^2$
	$5snd^3D_3$	$15 \leq n \leq 45$	2.52(2)	$1.0(2) \times 10^2$	$-6.1(8) \times 10^4$
	$5snd^3D_2$	$16 \leq n \leq 50$	2.6548(5)	$-1.10(7) \times 10^1$	$-8.9(2) \times 10^3$
	$5snd^3D_1$	$18 \leq n \leq 32$	2.67(7)	$-0(1) \times 10^2$	$-1(3) \times 10^4$
$L = 3$	$5snf^1F_3$	$5 \leq n \leq 21$	0.0841(2)	-1.05(7)	$-1.6(5) \times 10^1$
	$5snf^3F_4$	$4 \leq n \leq 28$	0.113(1)	-0.5(1)	2(2)
	$5snf^3F_3$	$4 \leq n \leq 28$	0.113(1)	-0.4(1)	1(2)
	$5snf^3F_2$	$4 \leq n \leq 28$	0.112(1)	-0.4(1)	1(2)

it necessary to fit measured values using the Rydberg-Ritz formula shown in equation (4.2). In the scope of this work all known measurements and calculations of quantum defects in  $^{88}\text{Sr}$  were combined in one database to enable a quick access in the further calculations. The data tables are listed in Appendix A.1. With this set of data it is quite simple to obtain fitting parameters for equation (4.2). The plots, showing the quantum defects and the fit itself, are shown in figure 4.2. Obtained quantum defects with the used  $n$ -range are listed in table 4.1. The collected data represent the basis of further calculations since it combines all deviations of strontium in relation to one electron systems. The exact process of working with the calculated data is described in section 5.2.

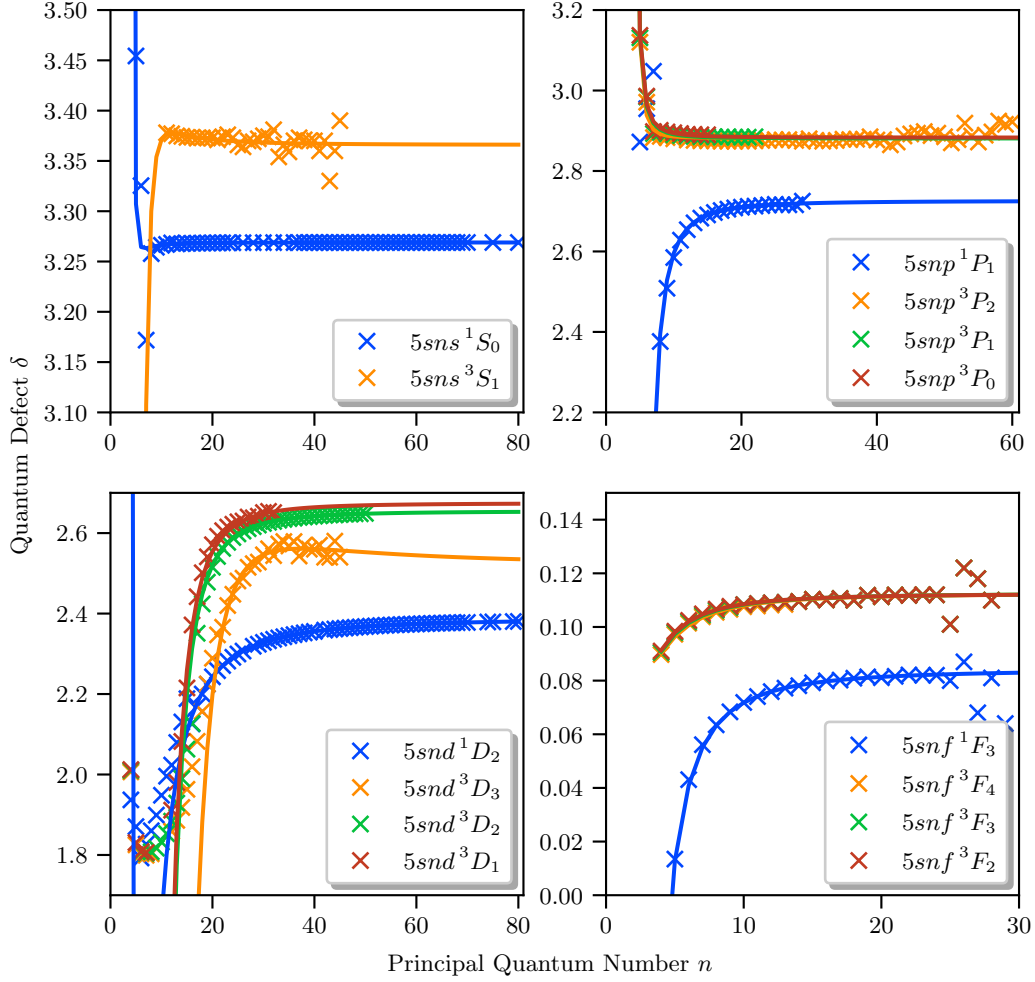


Figure 4.2.: Plot of the quantum defect data listed in table A.2, A.3 and A.4. States with the same angular momentum quantum number are plotted in the same panel, to give a better impression of the quantum defect regime. It can be seen that the quantum defect decreases for higher  $L$  which leads to a hydrogen-like situation for high  $L$  states. Also visible is the difference between singlet and triplet states. The quantum defects of triplet states with the same angular momentum quantum number often converge for higher principal quantum numbers, however the singlet state never combines with the triplet states.

The data for every state was fitted with a function of the form of equation (4.2) to obtain  $n$  dependent quantum defect formulations. The obtained fit data is listed in table 4.1.

### 4.3. Error Compensation in the Coulomb Approximation

As mentioned in section 3.2, the input of quantum defects in the Schrödinger equation prevents errors in the state energies and wavefunctions occurring due to potential approximations. To discuss this one has to check which errors are expected to occur. Therefore it should already be anticipated that the approximation will neglect core polarizability terms and will only consist of a Coulomb potential. This means that the quantum defect must give accurate parameters for all Rydberg-Ritz-Coefficients in equation (4.2). As it can be seen in table 4.1, fit values were obtained up to a good accuracy for principal quantum numbers larger as ten in average. Using the  $\delta_2$  and  $\delta_4$  coefficients in all calculations can, as described in section 4.1.2, compensate for the not included polarization effects. Here one has to be careful not to overestimate this capability: Core polarizability effects are mostly present in regions with small  $r$ . Since  $r$  scales with  $n^2$ , this means that quantum defects have to be the most accurate at small  $n$ . This cannot be achieved since the second valence electron largely affects the measured defects in this area, as can be seen in figure 4.2. Therefore the only solution is to cut off the whole  $n$  regime below the fitted area at approximately  $n = 15$ , which is below the mentioned  $n = 20$  limit of Rydberg states.

Regarding Rydberg states one also has to ask if the accuracy for high  $n$  is good enough. Therefore it is helpful to compare the data to other work. For this purpose calculated deviations are listed in table 4.2. The largest deviations can be observed for the  $^3D_3$  and the

Table 4.2.: List of reference values (Ref. Val.) for the  $\delta_0$  coefficient in equation (4.2) [47] and the deviation (Dev.) of the values obtained in the scope of this work to the reference.

State	Ref. Val. $\delta_0$	Dev. (%)	State	Ref. Val. $\delta_0$	Dev. (%)
$5sns^1S_0$	3.26896(2)	$5.2922 \times 10^{-4}$	$5snd^3D_2$	2.636(5)	$-7.13202 \times 10^{-1}$
$5sns^3S_1$	3.371(2)	$1.48324 \times 10^{-1}$	$5snd^3D_1$	2.658(6)	$-4.51467 \times 10^{-1}$
$5snp^1P_1$	2.7295(7)	$1.28229 \times 10^{-1}$	$5snf^1F_3$	0.089(1)	5.50562
$5snp^3P_2$	2.8719(2)	$-3.51684 \times 10^{-1}$	$5snf^3F_4$	0.12(1)	5.83333
$5snp^3P_1$	2.8824(2)	$4.85706 \times 10^{-2}$	$5snf^3F_3$	0.12(1)	5.83333
$5snp^3P_0$	2.8866(1)	$1.24714 \times 10^{-1}$	$5snf^3F_2$	0.12(1)	6.66667
$5snd^1D_2$	2.3807(2)	$-2.99492 \times 10^{-1}$			
$5snd^3D_3$	2.63(1)	4.18251			

$F$  states and are in the range of 5%. Those deviations could occur because the lower end of the fitting range is smaller in this work compared to the reference. Also the accuracy of the coefficients themselves plays a role since the reference values are given with only three significant digits. Considering these factors it still can be assumed that the values in table 4.1 are accurate enough if one takes care by calculating the states mentioned.

In summary it is expected that the quantum defects obtained by fit parameters should be accurate enough to compensate errors occurring due to the Coulomb approximation. To underline the statements of this section there will be further test calculations in the next chapter. Also the obtained final results will give a further possibility to discuss, if the approach using quantum defects is as accurate as expected.



## 5. Coulomb Approximation

Since the model potential approach comes with many further problems, it is necessary to find a simpler approach which still solves the problem with a satisfying accuracy. In this chapter a final approach combining potential approximations and quantum defect theory will be discussed and implemented. Also limitations of the approach are mentioned and examined.

### 5.1. Idea of the Approximation

As already mentioned in section 3.1, the potential of the Rydberg electron has the general form

$$V(r) = -\frac{1}{r} - \frac{\alpha_c}{r^4} \quad (5.1)$$

where the first term denotes the Coulomb potential and the second term considers the effect of the core polarizability  $\alpha$ . The idea now is to neglect the second potential term to be left with the so-called Coulomb approximation of the potential. This step seems tough but it will be shown that the obtained results of this method are good for Rydberg states. This is very helpful, since this approximation gives the possibility to address the strontium atom nearly hydrogen-like for Rydberg states.

The goal of the approximation is to obtain a new differential equation which can be solved numerically with little effort. As the only potential term is a Coulomb potential after the approximation it is possible to simplify to the Coulomb equation of the hydrogen case as described in section 2.2.1. By including the reduced mass  $\mu$  this equation is now given as

$$\left[ -\frac{d^2}{dr^2} + \frac{l(l+1)}{r^2} - \frac{2\mu}{r} \right] u_{E,l}(r) = 2\mu E u_{E,l}(r) \quad (5.2)$$

where the notation of C. L. Vaillant is used because his work [47, 48] gives the frame for the following calculations. Equation (5.2) is expected to return the radial wavefunctions when precise energies are used. At this point it is important to not ignore the errors obtained by the approximation. In the following an appraisal of the accuracy will be done to validate the Coulomb equation.

As mentioned in section 4.3, the quantum defect input into the Schrödinger equation should compensate errors occurring due to the approximation. Especially the core polarizability is expected to be obtained quite accurate if quantum defects with good accuracy are used. This guess must be tested by actual calculations.

Calculated values for comparison can be found in the already mentioned work of C. L. Vaillant [48]. Sadly, all calculations have just been done for rubidium which as an alkali atom just represents the one-electron problem. Since there are no available values calculated for strontium by more sophisticated means like multichannel quantum defect theory or a model potential approach, the comparison with rubidium must be satisfactory. Here it has to be differentiated between high  $n$  and low  $n$  regimes since ground states are much more affected by core polarizability effect. For the ground state transitions it is possible to directly compare

Table 5.1.: Comparison between oscillator strengths of transitions in rubidium obtained by using a quantum defect approach and literature values. The quantum defect approach uses a Coulomb approximation of the atom potential. All values listed are taken from [48, p. 26]. The reference values were taken out of [49].

Transition	QDT Value	Reference Value	Difference [%]
$5 S_{\frac{1}{2}} \rightarrow 5 P_{\frac{1}{2}}$	0.347	0.3456	0.5
$5 S_{\frac{1}{2}} \rightarrow 5 P_{\frac{3}{2}}$	0.703	0.7015	0.3
$7 S_{\frac{1}{2}} \rightarrow 8 P_{\frac{1}{2}}$	0.0189	0.0185	2.2
$7 S_{\frac{1}{2}} \rightarrow 8 P_{\frac{3}{2}}$	0.0436	0.0428	2.0
$5 P_{\frac{1}{2}} \rightarrow 7 D_{\frac{3}{2}}$	0.0163	0.01711	4.4
$5 P_{\frac{3}{2}} \rightarrow 7 D_{\frac{3}{2}}$	0.00176	0.00186	5.3
$5 P_{\frac{3}{2}} \rightarrow 7 D_{\frac{5}{2}}$	0.0157	0.01657	5.2
$4 D_{\frac{3}{2}} \rightarrow 5 P_{\frac{1}{2}}$	0.304	0.3324	8.5
$4 D_{\frac{3}{2}} \rightarrow 5 P_{\frac{3}{2}}$	0.0605	0.0654	7.5
$4 D_{\frac{3}{2}} \rightarrow 7 P_{\frac{1}{2}}$	0.0118	0.0077	54.4
$4 D_{\frac{3}{2}} \rightarrow 7 P_{\frac{3}{2}}$	0.00233	0.0015	51.7
$5 D_{\frac{3}{2}} \rightarrow 6 P_{\frac{3}{2}}$	0.0989	0.0975	1.4
$5 D_{\frac{5}{2}} \rightarrow 6 P_{\frac{3}{2}}$	0.594	0.5864	1.3

matrix elements in the form of oscillator strengths. This comparison is listed in table 5.1. It can easily be seen that the Coulomb approximation does not work for each transition but it is in good agreement for most of the cases. Regarding the low  $n$  regime which is looked at this is surprising. The largest errors at the transitions  $4 D_{\frac{3}{2}} \rightarrow 7 P_{\frac{1}{2}}$  and  $4 D_{\frac{3}{2}} \rightarrow 7 P_{\frac{3}{2}}$  can be traced back to the fact, that the effective quantum number  $n_{\text{eff}}$  of  $4 D_j$  is close to the angular momentum quantum number  $l$  which leads to problems due to the formulation of the Coulomb method [50]. These errors differ in their strength from 7.5% up to 54.4% where the lower end is still acceptable. But since in the few values no regularity can be seen it has to be assumed that the whole series lacks accuracy.

Up to this point there is no publication (to the author's knowledge) on Rydberg state dipole matrix elements in rubidium. Nevertheless it is important to compare the Coulomb approximation to literature values for all  $n$  regimes. One option is to compare radiative lifetimes which directly correspond to the dipole matrix elements via

$$\mathcal{D}_{ab} = \sqrt{\frac{3\pi\epsilon_0\hbar c^3}{\omega_{ba}^3}} \frac{1}{\Gamma_a^b} \quad (5.3)$$

where  $\mathcal{D}_{ab}$  denotes the matrix element itself,  $\omega_{ba}$  denotes the transition frequency and  $\Gamma_a^b = \tau_{ba}^{-1}$  denotes the rate of radiative decay. The lifetime values can be found for rubidium to expand table 5.1 to higher  $n$  regimes. Vaillant also included blackbody radiation effects to the calculated lifetimes and then plotted both calculated and experimental values in a graph shown in figure 5.1. As it can be seen in the graph also for high  $n$  values the Coulomb approximation gives quite good results for the lifetimes and therefore also the dipole matrix elements for the  $n S_{\frac{1}{2}}$  and  $n D_{\frac{5}{2}}$  states. Problems occur for the  $n P_{\frac{3}{2}}$  states where Vaillant assumes that the strong coupling to the  $4 D_j$  states, which show large inaccuracies, is the cause. The errors for these states were already mentioned above.

To summarize the considerations it can be said that it is very difficult to make assumptions about the accuracy of the approximation. There are many reference values for alkali atoms,

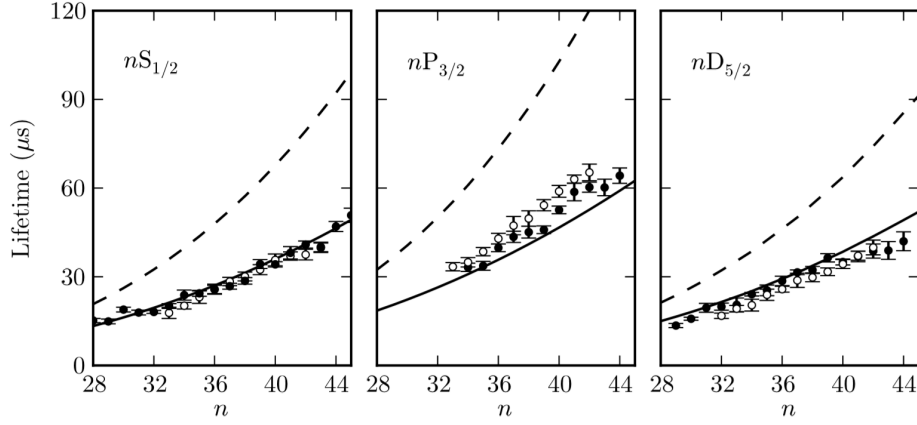


Figure 5.1.: Plots of rubidium lifetimes obtained by quantum defect theory (QDT) calculation and experimental values. The dashed lines are the QDT values without blackbody radiation, solid lines include blackbody radiation and the experimental data sets are pictured as closed and open symbols. The figure was taken from [48, p. 33].

especially for rubidium, but just calculated values for strontium. Since it cannot be concluded that an approximation works for two-electron atoms just by testing it on one-electron atoms the preliminary considerations can just give a vague idea of the actual accuracy of the model. Later in this work, the obtained results will also be cross checked with other calculation methods to assure a validation not just based on the assumptions made above.

## 5.2. Python Implementation

This section will focus on explaining the python implementation of calculating radial wavefunctions and dipole matrix elements. For this purpose the three modules *sr\_state\_properties.py*, *sr\_wavefunction.py* and *sr\_dipolematrixelement.py* are described and an implementation example for the modules is given. In the following all calculations are implemented in Hartree atomic units.

### 5.2.1. Characterize Strontium States: *sr\_state\_properties.py*

The general goal is to solve equation (5.2) numerically. This equation is dependent on the eigenenergy of atomic states, the angular momentum quantum number  $L$  and the reduced mass  $\mu$ . To distinguish the energy it is necessary to use the quantum defects determined in section 4.2. The other dependencies are either defined by the state definition or are constant. To gather all parameters needed to solve the Coulomb equation, a class named *strontium\_state* is defined. This class combines the two functions *get\_Quantumdefect* and *calc\_Stateproperties*. Both functions are working with the class wide defined input variables  $n$ ,  $S$ ,  $L$  and  $J$  which precisely define one strontium state. The function *get\_Quantumdefect* converts a database *Fitdata\_QuantumDefects.csv*, which stores all values listed in table 4.1, into numpy arrays and returns the data for the specified quantum numbers. This data is then passed to *calc\_Stateproperties*, where the quantum defect  $\delta$ , the effective principal quantum number  $n_{\text{eff}} = n - \delta$  and the eigenenergy  $E$  via equation (4.1) are calculated. The constants used in the calculations are imported from the *scipy.constants* module. The Rydberg constant is defined as  $R_{\text{Sr}} = 109\,736.627\text{ cm}^{-1}$  following [51]. Furthermore the effective mass of strontium is defined in atomic units as

$$\mu = \frac{m_{\text{Sr88}}^{\text{a.u.}}}{m_{\text{Sr88}}^{\text{a.u.}} + 1} \quad (5.4)$$

where the mass of strontium is  $m_{\text{Sr88}}^{\text{a.u.}} = 160242.12798792866 m_e$  [52].

With this set of variables it is possible to implement the wavefunction calculation itself. Since all variables are defined as attributes of *strontium\_state* they can easily be called by importing the class and setting its initial parameters as can be seen in section 5.2.4.

### 5.2.2. Calculate Radial Wavefunctions: *sr\_wavefunction.py*

This module implements the calculation of radial wavefunctions by solving the Coulomb equation (5.2) with a Numerov algorithm [29]. The solving algorithm itself is a straight forward calculation which follows section 2.2.3. In the following section just the important frame aspects of the implementation will be commented on.

Even though it is not necessary the wavefunction calculation works best if it is combined with the class *strontium\_state*. If this class is not used one needs to define the input parameters separately which would be useful when other elements than strontium are calculated. Since this is not included in the scope of this work, this section is limited to the calculation of strontium wavefunctions. In this case of use it is not necessary to define parameters when using the class *strontium\_wavefunction*. If implemented correctly, all arguments of the function, namely  $n$ ,  $L$ ,  $n_{\text{eff}}$ ,  $\mu$ ,  $E$  and *state\_variables*, are imported from *strontium\_state*. The calculation itself is introduced by the function *calc\_radialWavefunction*.

Most important to discuss are two of the optional arguments in *calc\_radialWavefunction*, namely  $r_{\text{min}}$  and  $r_{\text{max}}$ . They define the inner and outer turning point of the integration. If set manually, those parameters can lead to a diverging wavefunction at  $r \rightarrow 0$ . This effect

arises because the Coulomb equation is solved by calculating inwards. The outer turning point  $r_{\max}$  should lie further out than the last maximum of the wavefunction, where it is decayed to almost zero, to not cut parts of the solution. Besides this condition it can theoretically be chosen arbitrarily at some point  $r_{\max} \rightarrow \infty$ .

For the inner turning point  $r_{\min}$  harder conditions are required. It is possible to guess values for the turning point but this is time-consuming and not very effective. Therefore the inner turning point is defined as

$$r_{\min} = n_{\text{eff}}^2 \left[ 1 - \sqrt{1 - \frac{(L + 0.5)^2}{n_{\text{eff}}^2}} \right]. \quad (5.5)$$

This definition was proposed by Rudolph E. Langer [53] as this is also the definition of the classical turning points in a Coulomb potential. Accordingly it is possible to define the outer turning point as

$$r_{\max} = n_{\text{eff}}^2 \left[ 1 + \sqrt{1 - \frac{(L + 0.5)^2}{n_{\text{eff}}^2}} \right] \quad (5.6)$$

which is used if no other input is given to the function. This leads to a cutoff at the almost completely decayed outer end of the wavefunction.

These definitions are crucial, but not sufficient to hinder the wavefunction from diverging. Another critical aspect of the calculation is the choice of initial parameters. Proposed is a solution depending on the number of wavefunction slopes. This is implemented as follows:

```

1 if ((self.n-self.L) % 2)==0:
2     div_init=-1e-3
3 else:
4     div_init=1e-3
5
6 self.initial_values=[div_init,0]
```

The idea behind this solution can be understood graphically. For this purpose two different Coulomb functions are plotted in figure 5.2. The function displayed in figure 5.2a shows the state  $5s10s^1S_0$  for which the number of nodes gives an even number. For the state  $5s9s^1S_0$  shown in 5.2b on the other hand, the number of nodes  $\propto n - L$  gives an odd number. By knowing this correlation it is furthermore possible to make a statement about the slope at the outer turning point. To achieve a negative slope for  $r \rightarrow 0$  it is necessary that for even node numbers the slope is negative at  $r_{\max}$ . The opposite case is true for odd node numbers. To force this behavior the first initial condition set in the code snippet gives a small tendency to the second outmost point of the wavefunction. Additionally the initial values also include the continuity conditions at  $r \rightarrow \infty$  which assures a decay of the wavefunction when set to zero. Although parts of the initial conditions are only used for numerical purposes it is important to mention that the conditions are of a physical nature. As in every quantum mechanical calculation it is inevitable to satisfy continuity conditions of the wavefunction.

The methods preventing divergence and the initial conditions define most of the calculation. With them being already discussed in detail it is now possible to take a short look at the Numerov algorithm implementation. The algorithm only solves the Coulomb equation under all considerations mentioned above and returns the Coulomb function.

```

1 '''
2     Numerov Method Implementation as an Inward Integration
3 '''
4 def numerov(r,dr,V,E,initial_values):
```

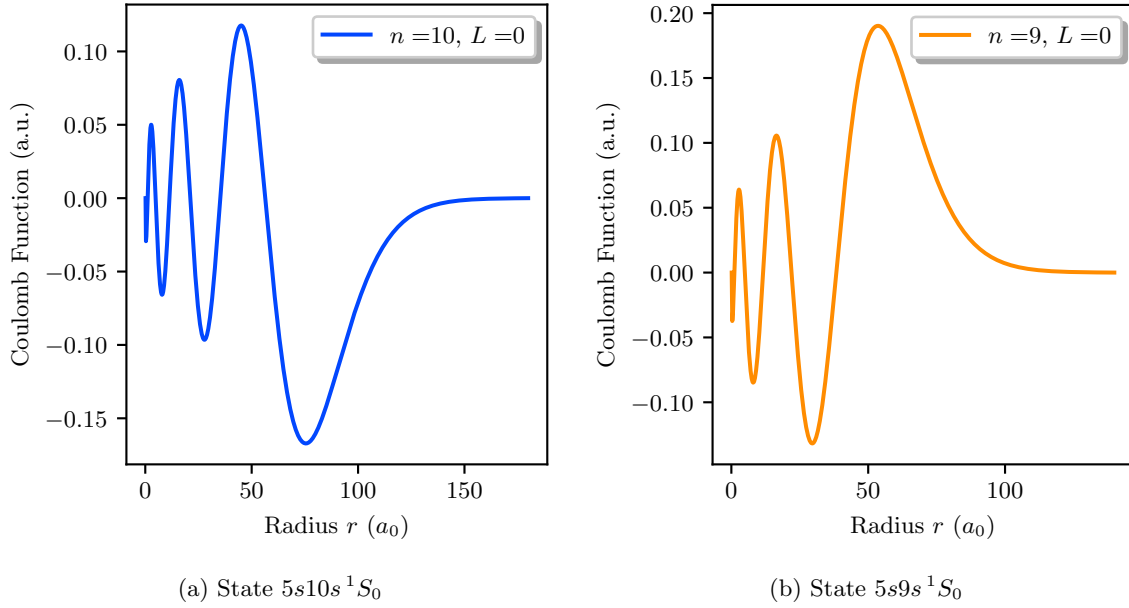


Figure 5.2.: Plot of the Coulomb functions  $u(r) = rR(r)$  for the two states  $5s10s^1S_0$  and  $5s9s^1S_0$ . It can be seen that the number of nodes and therefore the initial conditions of the wavefunctions depend on the difference  $n - L$ . Further details are given in the text.

```

5  steps = r.shape[0]-1
6  coulomb_function = np.zeros(steps+1)
7  coulomb_function[steps-1:steps+1] = initial_values
8
9  def g(n):
10     return (V(r[n])+2*self.mu*self.E)
11
12  for i in range(steps-1,1,-1):
13     coulomb_function[i-1] = (2*coulomb_function[i]*(1-
14         (5/12)*dr**2 *g(i))-coulomb_function[i+1] \
15         *(1+ (1/12)*dr**2 *g(i+1)))/(1+(1/12)*dr**2 *g(i-1))
16
17  return coulomb_function

```

The turning points discussed above are taken into account via the definition of the radial coordinate  $r$  as a discrete array

```

1 self.r = np.arange(self.r_min, self.r_max, self.dr)

```

which is from now on always used as the calculation basis.

The returned Coulomb function resembles the radial wavefunction after resubstitution. It is mandatory to define a norm of the radial wavefunction. The normalized function is defined as

$$R_{\text{norm}}(r) = \frac{R(r)}{\int_{r_{\text{min}}}^{r_{\text{max}}} |R(r)|^2 r^2 dr} \quad (5.7)$$

where the integral is implemented as the sum over the array of the radial coordinate  $r$ . Furthermore the normalized Coulomb function is defined as

$$u_{\text{norm}}(r) = rR_{\text{norm}}(r). \quad (5.8)$$

Both functions are returned by the *calc\_radialWavefunction* function via

```

1 '''
2     Output of the Solution gives Coulomb Function and Radial
3     Wavefunction
4 '''
5 self.coulomb_function = numerov(self.r,self.dr,V,self.E,self.
6     initial_values)
7 self.radial_Wavefunction = self.coulomb_function/self.r
8 '''
9     Normalization of the Radial Wavefunction
10 '''
11 self.norm_radial = np.sqrt(np.sum(self.radial_Wavefunction**2 *self.r**2
12     *self.dr))
13 self.radial_Wavefunction_norm = self.radial_Wavefunction/self.
14     norm_radial
15 self.coulomb_function_norm = self.r*self.radial_Wavefunction_norm
16 return self.coulomb_function, self.coulomb_function_norm, self.
17     radial_Wavefunction, self.radial_Wavefunction_norm

```

### 5.2.3. Calculate Dipole Matrix Elements: *sr\_dipolematrixelement.py*

The calculation of dipole matrix elements follows section 2.3.2 where all steps are described with their physical background. In the following the class *strontium\_dipolematrixelement* should be described in detail to understand how every step is implemented separately. This class relies on the *strontium\_state* class as well as on the *strontium\_wavefunction* class since the dipole matrix elements are calculated using radial wavefunctions for two different states. Therefore an implementation of the *strontium\_dipolematrixelement* class also includes the other two modules. Alternatively one can also calculate dipole matrix elements out of existing wavefunctions. In this case the other modules are imported but not used.

Since dipole matrix elements always describe transitions between two states, it is necessary to input two sets of quantum numbers. This includes all four state defining quantum numbers  $n$ ,  $S$ ,  $L$  and  $J$ . To calculate state transitions the function *calc\_radialDipolematrixelement* starts by importing the state properties of both states. This is implemented via calling the class *strontium\_state* respectively for each state. To calculate the radial wavefunctions, a commonly used array for the radial coordinate must be defined. Even though this is not inevitable for the calculation itself, it becomes important when calculating the dipole matrix element, since a numerical integration over two different arrays is not possible. By defining this array one has to be careful to not cut off parts of the radial wavefunctions or cause a divergence at  $r \rightarrow 0$ . To assure that this will not happen, the array range is defined by the largest  $r_{\min}$  and  $r_{\max}$  via

```

1 r_min_state1 = self.state1.n_eff**2 *(1-np.sqrt(1-(self.state1.L+5)**2/
2     self.state1.n_eff**2))
3 r_max_state1 = self.state1.n_eff**2 *(1+np.sqrt(1-(self.state1.L+5)**2/
4     self.state1.n_eff**2))
5 r_min_state2 = self.state2.n_eff**2 *(1-np.sqrt(1-(self.state2.L+5)**2/
6     self.state2.n_eff**2))
7 r_max_state2 = self.state2.n_eff**2 *(1+np.sqrt(1-(self.state2.L+5)**2/
8     self.state2.n_eff**2))
9
10 if r_min_state1 > r_min_state2:
11     r_min = r_min_state1
12 else:

```

```

9         r_min = r_min_state2
10
11     if r_max_state1 > r_max_state2:
12         r_max = r_max_state1
13     else:
14         r_max = r_max_state2

```

where *state1* and *state2* relate to the state properties of both states defined by *strontium.state*. The so defined inner and outer turning points are used as input variables in the *calc\_radialWavefunction* function of *strontium\_wavefunction*. Furthermore the step size *dr* is defined by the input variables of the class for both wavefunctions. These confinements now allow easy calculations using the array

```

1 self.r = np.arange(r_min, r_max, self.dr)

```

for all needs.

It is also possible to calculate the radial dipole matrix elements out of precalculated wavefunctions. This is implemented by the function *calc\_radialDME\_precalcWF*. This tool does have a few constraints: The wavefunctions have to be arrays with the same length and step size. Furthermore the start- and endpoints, namely  $r_{\min}$  and  $r_{\max}$ , must be identical for both arrays. If those constraints are defined as input arguments, the radial dipole matrix element can easily be calculated out of two *.npy* files.

The calculation of the total dipole matrix element is separated into three steps which are further discussed in section 2.3.2. In this chapter there will only be a short comment on the calculation to not go beyond the scope of the implementation documentation. As a first input, the radial dipole matrix element is calculated via

$$\mathcal{R}_{n_1L_1 \rightarrow n_2L_2} = \int_{r_{\min}}^{r_{\max}} R_{n_1,L_1}(r) r R_{n_2,L_2}(r) r^2 dr \quad (5.9)$$

from the radial wavefunctions. Here the normalized wavefunctions are used, but the index is neglected for the sake of clarity.

For further calculations an implementation of Wigner symbols is needed. Since there is a functioning implementation in the Alkali Rydberg Calculator (ARC) [28] there was no need to design another. To still have an alternative method, it is also possible to choose the Wigner symbols provided by the sympy package. Both methods are stored in *wigner.py* where the ARC code is embedded as complete code to be independent of changes.

The Wigner symbols are now used to implement reduced dipole matrix elements and fine structure effects. These calculations are defined in the function *calc\_angularDipolematrixelement* listed below.

```

1 def calc_angularDipolematrixelement(self):
2     '''
3         Calculates the angular dipole matrix element between two
4         states using Wigner symbols.
5         The Wigner symbols are defined in 'wigner.py'. There are
6         two methods available:
7         1) Calculation via ARC code
8         2) Calculation via Sympy
9         Both methods are working equally good.
10
11        Returns:
12            reduced_DME_L (float): reduced dipole matrix
13                element
14            reduced_DME_J (float): reduced dipole matrix
15                element in the fine structure basis

```

```

12     '''
13     '''
14     Calculation of the reduced dipole matrix element.
15     '''
16     def calc_reduced_DME_L(self):
17         reduced_DME_L = (-1)**(self.L1) *np.sqrt((2*self.L1+1)
18             *(2*self.L2+1)) \
19             *ARC_Wigner3j(self.L1, 1,self.L2,0,0,0) \
20             *self.radial_Dipolematricelement
21         return reduced_DME_L
22
23     self.reduced_DME_L = calc_reduced_DME_L(self)
24
25     '''
26     Manual implementation of the selection rule 'delta S=0'
27     to make sure, that singlet and triplet
28     series are treated separately and no spin flip processes
29     occure. This is justified only for rydberg atoms,
30     but since the whole wavefunction calculation is only
31     suited for high n-states this assumption is valid.
32     '''
33     if self.S1 == self.S2:
34         self.S = self.S1
35         self.selection_rule_S = 1
36     else:
37         self.S=0
38         print("Error: Calculation not possible. The condition S1
39             =S2 must be satisfied.")
40         self.selection_rule_S = 0
41
42     '''
43     Calculation of the reduced dipole matrix element in the
44     fine structure basis.
45     '''
46     def calc_reduced_DME_J(self):
47         reduced_DME_J = (-1)**(int(self.L1+self.S+self.J2+1)) \
48             *np.sqrt((2*J1+1)*(2*J2+1)) \
49             *ARC_Wigner6j(self.J1,1,self.J2,self.L2,self.S,
50                 self.L1) \
51             *self.reduced_DME_L \
52             *self.selection_rule_S
53         return reduced_DME_J
54
55     self.reduced_DME_J = calc_reduced_DME_J(self)
56
57     return self.reduced_DME_L , self.reduced_DME_J

```

The calculation is relatively straightforward. The idea for the implementation of the basis change was taken from [28]. To ensure correct calculation of dipole matrix elements, a manual implementation of the selection rule  $\Delta S = 0$  was included. This separates the singlet and triplet series which can be motivated by the fact that transitions between these series are weak compared to transitions inside the series. To check this behavior one can compare Einstein coefficients for spontaneous emission which are proportional to the absolute value squared of the reduced dipole matrix element. To give examples, the  $5s4d^1D_2 \rightarrow 5s6p^1P_1$  transition has an Einstein coefficient of  $A_{ij} = 9.4(19) \times 10^6 \text{ s}^{-1}$  where the  $5s4d^1D_2 \rightarrow 5s6p^3P_2$  transitions only has a coefficient of  $A_{ij} = 6.0(12) \times 10^6 \text{ s}^{-1}$ . For the  $5s4d^1D_2 \rightarrow 5s6p^3P_1$  transition the coefficient reaches  $A_{ij} = 1.6(3) \times 10^6 \text{ s}^{-1}$ . For other transitions the effect gets even larger. The transition  $5s4d^3D_1 \rightarrow 5s6p^1P_1$  features an Einstein coefficient of  $A_{ij} = 1.4(3) \times 10^4 \text{ s}^{-1}$  which is smaller by a factor of  $10^2$  compared to the  $5s4d^3D_1 \rightarrow 5s6p^3P_1$  transition with  $A_{ij} = 3.7(8) \times 10^6 \text{ s}^{-1}$ . All of the values are taken from [52]. This selection rule is just valid

for dipole transitions and must be abandoned for higher order transitions which are, however, currently not implemented in the software.

A resulting reduced dipole matrix element in the fine structure basis can be converted into the resulting dipole matrix element by using the Wigner-Eckart theorem following section 2.3.2. This is done in the `calc_Dipolematrixelement` function which requires an additional input of the total angular momentum quantum number projection  $m_J$  of both states. Furthermore an additional parameter  $q$  specifies the transition driven by light with  $\pi$  or  $\sigma^\pm$  polarisation. For those cases one has to set the parameter to  $q = 0$  and  $q = \pm 1$ . The additional parameters are put into the calculation shown below.

```

1 self.Dipolematrixelement = (-1)**(int(self.J1-self.M_J1)) \
2   *ARC_Wigner3j(self.J1,1,self.J2,-self.M_J1,-self.q,self.M_J2) \
3   *self.reduced_DME_J

```

The resulting dipole matrix element contains all selection rules for electric dipole transitions.

### 5.2.4. Implementation Example

As the implementation of the Coulomb approximation approach is done via classes, it is necessary to programm a small frame to access all features. In this paragraph two minimal examples should be given to show which functions have to be called. All information about the functions can be found above. Since this is just about the program usage, no further explanations will be given.

#### Single State Wavefunction

```

1 from sr_state_properties import strontium_state
2 from sr_wavefunction import strontium_wavefunction
3
4 '''
5     Loading a single state with quantum defect data.
6 '''
7 state = strontium_state(n,S,L,J)           #calling the class
8 state_QD = state.get_Quantumdefect()      #calculate QD
9 state_prop = state.calc_Stateproperties()  #calculate energy etc
10
11 '''
12     Calculate the radial wavefunction of the loaded state.
13     Abbreviations:
14         WF - (radial) wavefunction (normalized)
15         CF - Coulomb function (normalized)
16 '''
17 init_radial_Wavefunction = strontium_wavefunction(state_variables=state)
18                               #calling the class
19 calc_radial_Wavefunction = init_radial_Wavefunction.
20                               calc_radialWavefunction(r_min,r_max,dr) #calculate radial WF
21 WF = init_radial_Wavefunction.radial_Wavefunction_norm #ouput WF array
22 CF = init_radial_Wavefunction.coulomb_function_norm    #ouput CF array

```

#### Dipole Matrix Element

```

1 from sr_dipolematrixelement import strontium_dipolematrixelement
2
3 '''
4     The DME class automatically loads two states and WFs.
5     Abbreviations:
6         DME - dipole matrix element

```

```
7         WF - (radial) wavefunction (normalized)
8     '''
9     init_DME = strontium_dipolematricelement(n1,S1,L1,J1,n2,S2,L2,J2,dr)
10         #calling the class
11 'First option: Calculating WFs and DME'
12 radial_DME = init_DME.calc_radialDipolematricelement()
13 'Second option: Use precalculated WFs to calculate DME'
14 radial_DME = init_DME.calc_radialDME_precalcWF(state1_file,state2_file,
15         r_min,r_max,dr)
16 angular_DME = init_DME.calc_angularDipolematricelement()
17         #calculating reduced DME
18 total_DME = init_DME.calc_Dipolematricelement(M_J1,M_J2,q)
19         #calculate total DME
```

### 5.3. Limitations

The Coulomb approximation itself and also the Python implementation have their limitations. It is important to be aware of both physical and numerical limits to avoid errors in calculations. This section should give an overview and a quick discussion on all known restrictions.

#### 5.3.1. Physical Limitations

Every approximation is limited to certain aspects of a problem. The Coulomb approximation is no exception. To determine the physical limits, two influences have to be considered: First the atom potential and second the effects of the core. Those two influences will be discussed briefly in this section. More detailed informations about the general background of the factors can be found in chapters 3 and 4.

#### Atom Potential

The atom potential is the most obvious limitation to be discussed, as the simplest form of an atomic potential is used in the approach. Without including the quantum defects in the calculation, the problem would just consist of the well known hydrogen case.

To motivate the used potential it is helpful to compare it to other approaches. Since there are no one-dimensional model potentials for strontium (to the author's knowledge) the alkali atom  $^{87}\text{Rb}$  is used in the further discussion. In figure 5.3 one can see the Coulomb potential in comparison to a model potential from [40]. This potential has the form

$$V_{\text{model}} = V_{\text{S}}(r) + V_{\text{Pol}}(r) + V_{\text{s.o.}}(r) \quad (5.10)$$

where  $V_{\text{S}}(r)$  denotes the screened Coulomb term

$$V_{\text{S}}(r) = \frac{1}{r} \left[ 1 + (Z - 1) e^{-a_1 r} - r(a_3 + a_4 r) e^{-a_2 r} \right] \quad (5.11)$$

$V_{\text{Pol}}(r)$  the core polarizability term

$$V_{\text{Pol}}(r) = -\frac{\alpha_c}{2r^4} \left[ 1 - e^{-\left(\frac{r}{r_c}\right)^6} \right] \quad (5.12)$$

and  $V_{\text{s.o.}}(r)$  the fine structure term

$$V_{\text{s.o.}}(r) = \frac{\alpha_c^2}{4r^3} (J(J + 1) - L(L + 1) - S(S + 1)). \quad (5.13)$$

The constants used are the nuclear charge  $Z$ , the empirical obtained model parameters  $a_i$  ( $i = 1, 2, 3, 4$ ), the core dipole polarizability  $\alpha_c$ , the effective core size  $r_c$  and the fine structure constant  $\alpha$ .

In the plot of both potentials it can be seen that the difference vanishes for approximately  $5 \leq r < \infty$ . In this regime the Coulomb potential is expected to be a good approximation. Since here physical limits are discussed, it is important to note that smaller  $r$  are not covered with the Coulomb approach. This problem would be covered by better model potentials for strontium as it is implemented for rubidium. Those potentials must then be adapted individually for different positions of the second electron. This is possible in general but was not done yet and involves extensive numerics. The neglect of the term mentioned in equation (5.12) is directly correlated to the neglect of core effects. Those are briefly commented about below.

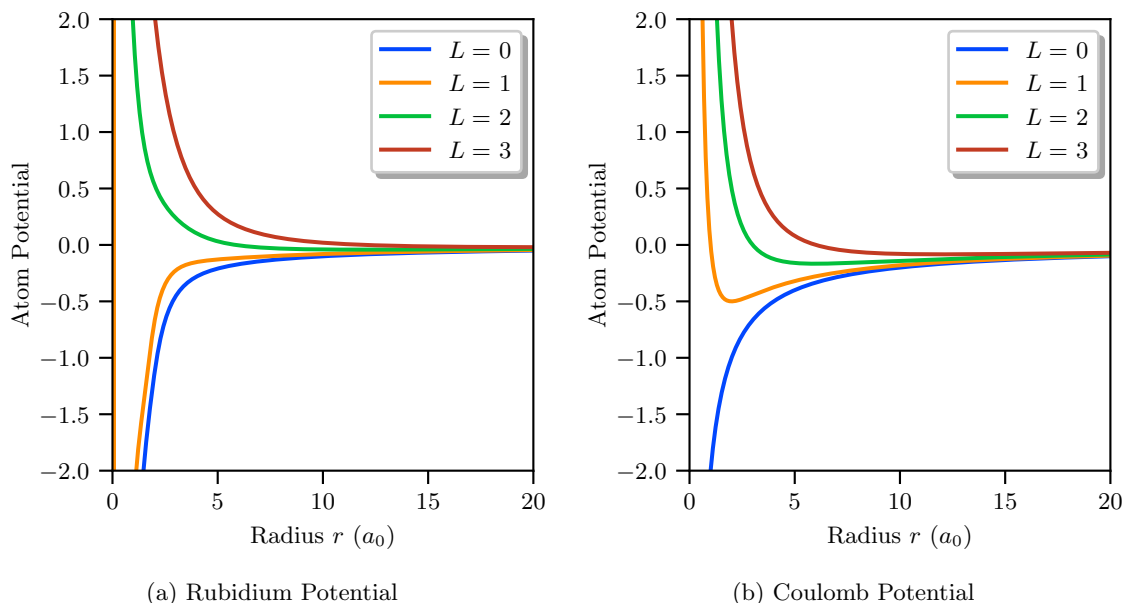


Figure 5.3.: Plot of a model potential for rubidium after (5.10) (fig. 5.3a) and the Coulomb potential used in the implementation (fig. 5.3b). On both potentials a centrifugal barrier term  $L(L+1)r^{-2}$  is added. Each potential is plotted for four different  $L$  values as listed in the legend. Differences are discussed in the text.

### Core Effects

As mentioned above the core effects directly influence the potential. In the Coulomb approximation the general idea is to treat the core as a point charge which is unaffected by the outer electrons. In the real atom this is of course not the case. The core has a finite size  $r_c$  as mentioned in equation (5.12) and a finite charge  $Z_{\text{eff}}$  which is influenced by core penetration effects of the electrons. This gives a state dependent variation of the potential problem which directly influences electron wavefunctions. By neglecting core effects one basically treats all electrons the same which is also a harsh approach at first. By using quantum defects as a disturbance for the eigenenergies it is possible to compensate the effects up to a certain degree. It has to be kept in mind that a quantum defect approach never replaces a good guess for atom potentials, so the model is limited regarding this problem.

### 5.3.2. Implementation Limitations

As described in section 5.2, the implementation mainly consists of a Numerov algorithm solving the Coulomb equation (5.2). This process requires a few steps to prevent wavefunction divergence. They lead to limitations of the application and numerical errors.

#### Influence of the Turning Points

The most important input in the Numerov method is the inner turning point  $r_{\text{min}}$  since it cuts off divergences at  $r \rightarrow 0$  and neglects areas where the Coulomb approximation would not be valid. As described in section 5.2.2, the turning point is defined by classical arguments. The formula used to determine the absolute value for each state depends on the effective principal quantum number  $n_{\text{eff}}$  and the angular momentum quantum number  $L$ . Whereas the dependence on  $n_{\text{eff}}$  is negligible, the  $L$  dependence has a huge influence on the value. For  $L \rightarrow \infty$  the inner turning point gets larger until it is not defined anymore. At this point it

equals the outer turning point. This behaviour is shown in figure 5.4. Additionally one can look at the Rydberg radius

$$\langle r \rangle = \frac{1}{2} [3n_{\text{eff}}^2 - L(L+1)] \quad (5.14)$$

which is defined as the orbit radius in Rydberg atoms [54].

As it can be seen in the plot, this radius also intersects with the turning points. The in-

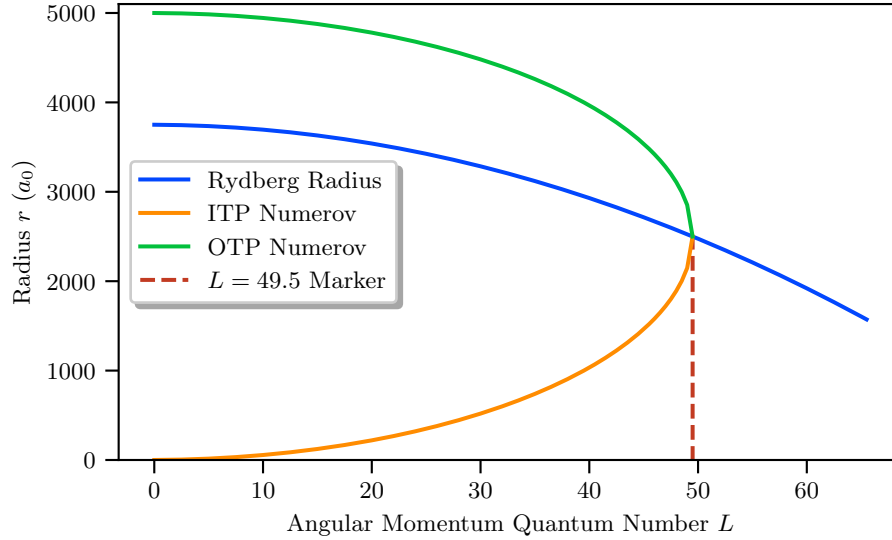


Figure 5.4.: Plot of the **Rydberg radius** (5.14) and the **inner/outer** turning points of the Numerov method over the angular momentum quantum number  $L$  at an effective principal quantum number of  $n_{\text{eff}} = 50$ . It can be seen that all three functions have a common point of intersection at  $L = 49.5$  marked by the **dashed line**. This impacts the solution method of the radial wavefunction as discussed in the text.

tersection itself is not problematic since the maximum  $L = n - 1 \approx n_{\text{eff}} - 1$  is below it. More of a problem is the shrinking calculation interval for high  $L$  states which makes the implementation unsuitable for circular Rydberg state calculations. In this regime just about half of the wavefunction would be present due to the inner turning point. This would affect the dipole matrix elements enormously.

For low  $L$  calculations on the other hand this limitation vanishes. Therefore in the calculations done in the scope of this work no problems with the turning points should occur.

### Influence of the Step Size

Although the step size does not have a physical meaning, it also influences the wavefunctions and thus the dipole matrix elements. To guarantee consistency it is necessary to confine all calculations on a certain resolution. To show the differences in a variety of resolutions, four different wavefunctions are plotted in figure 5.5. As it can be seen in the plot, the influence of the step size on the wavefunction shape vanishes for  $dr < 1$ . This limit seems very large since the wavefunction interval only has a size of approximately  $600 a_0$ . To double check this step size limit one can also calculate dipole matrix elements. For a  $\pi$ -transition of the  $5s20p^3P_2$

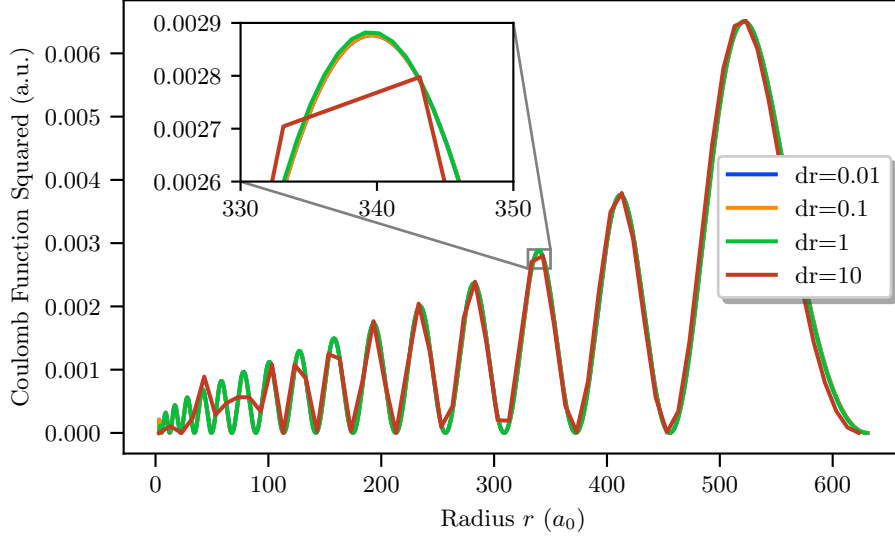


Figure 5.5.: Plots of the  $5s20p^3P_2$  wavefunction for different step sizes  $dr$ . The step size influences the calculation array  $r$  as described in section 5.2.2 and can therefore change the wavefunction and dipole matrix elements. This is discussed in detail in the text. The inset shows a more detailed view of the wavefunctions to get an idea about the differences caused by the step size.

state to the  $5s20d^2D_3$  state ( $m_{J_1} = 1 \rightarrow m_{J_2} = 1$ ) the dipole matrix elements

$$\begin{aligned}
 |\mathcal{D}|^{dr=10} & \approx 138.579 a_0 \\
 |\mathcal{D}|^{dr=1} & \approx 140.097 a_0 \\
 |\mathcal{D}|^{dr=0.1} & \approx 139.943 a_0 \\
 |\mathcal{D}|^{dr=0.01} & \approx 139.936 a_0 \\
 |\mathcal{D}|^{dr=0.001} & \approx 139.935 a_0
 \end{aligned}$$

can be calculated. All values are rounded to six significant digits. As it can be seen, the values differ largely for  $dr \geq 1$ . For lower  $dr$  the value seems to converge. Since the calculation of wavefunctions is very time costly for  $dr = 0.001$ , a  $dr$  of 0.01 is used for all calculations. This seems to be sufficient for dipole matrix calculations as it just differs by  $0.001 a_0$  in the values calculated above. By this choice, a good accuracy and efficiency can be achieved.

### Influence of the Initial Values

The numerical limitations discussed above directly influence the values of the wavefunctions and dipole matrix elements. The influence of the initial values on the other hand does not have any physical effects on the solution of the Coulomb equation since it only causes sign changes of  $R(r)$  and therefore  $\psi$  which are arbitrary. However, there is a dependency of the dipole matrix element sign which can be noticed when calculated values are compared to reference values. In figure 5.6 calculated dipole matrix elements and matrix elements of the Alkali Rydberg Calculator (ARC) [28] are plotted to illustrate this effect.

As it can be seen, the calculated values of the implementation are entirely negative whilst the ARC values change their sign for every  $n$  increase. The only sign dependence of the DME has its origin in the wavefunction respectively the integral of two wavefunctions. This integral is written as a sum because the wavefunctions are discrete arrays. The sign change is solely existent because the last slopes differ for different  $n$  values as shown in figure 5.7. It

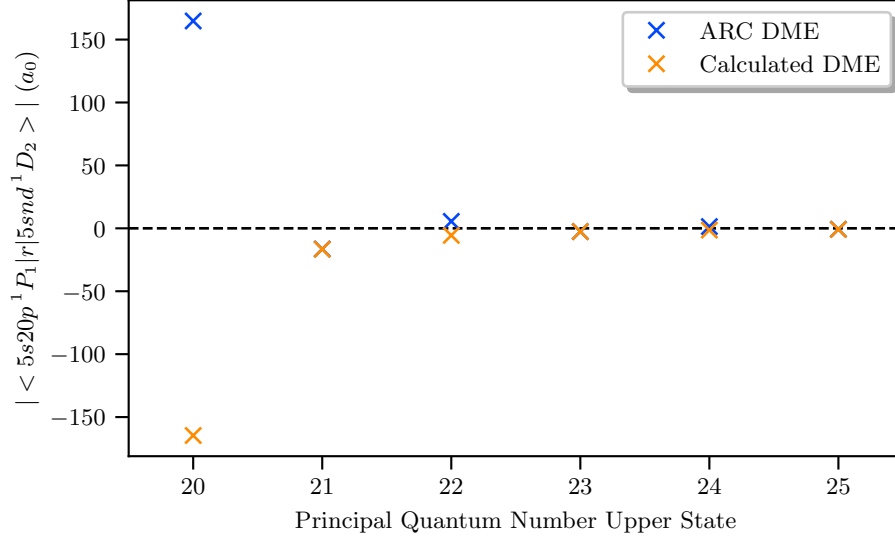
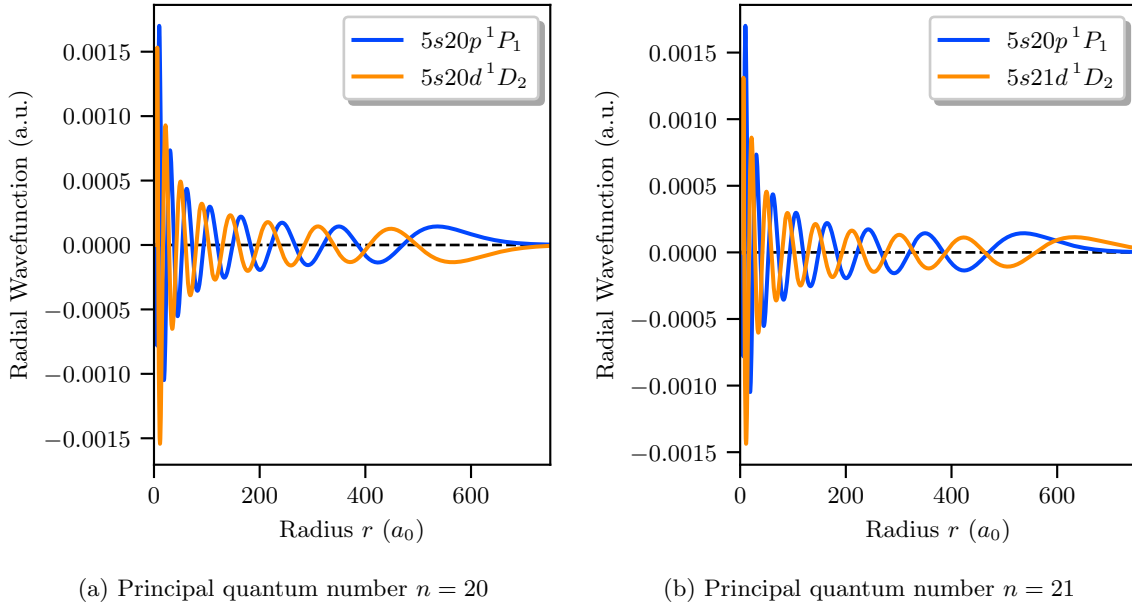


Figure 5.6.: Plots of the dipole matrix element between the states  $5s20p^1P_1$  and  $5snd^1D_2$  over the principal quantum number  $n$  of the second state. Here the  $\pi$ -transition from  $m_{J_1} = 1 \rightarrow m_{J_2} = 1$  is shown. To illustrate the influence of the initial values the **calculated dipole matrix elements** are compared with **dipole matrix elements** calculated with the ARC [28].



(a) Principal quantum number  $n = 20$

(b) Principal quantum number  $n = 21$

Figure 5.7.: Plot of the  $5s20p^1P_1$  and  $5snd^1D_2$  wavefunctions. The principal quantum number  $n$  is varied to show the sign change of the wavefunction. Further details are given in the text.

now depends on the initial values, which apply on the right side of the wavefunction, if the sum of both wavefunctions, ergo the integral, is positive or negative. In the implementation it is arbitrary chosen that both  $5snd^1D_2$  wavefunctions must end with the same slope at  $r \rightarrow 0$  by setting the initial values. It can not be physically motivated that the  $5s21d^1D_2$  wavefunction in figure 5.7b should not be inverted by multiplying with  $(-1)$  (which would be needed for a sign change in the DME).

This effect defines the sign of the dipole matrix element and leads to the difference pictured in figure 5.6. The error can not be avoided which makes it impossible to plot oscillating dipole matrix elements as in [29, p. 42] or in the ARC data. Since this is just a mathematical flaw which is not of physical nature, one can just use absolute dipole matrix elements.



## 6. Results and Discussion

With the Coulomb approximation described in chapter 5 it is possible to calculate wavefunctions (WF) and dipole matrix elements (DME) easily. This chapter will focus on the results of those calculations and a comparison to other methods, to set this work in context with other calculations and determine its shortcomings.

### Radial Wavefunctions

Radial wavefunctions for strontium are not readily available in literature. To still put the obtained values into context the “Pairinteraction” Rydberg calculator (PI) v0.9.4-alpha [27] is used to calculate reference functions. It is to note, that those results are also not experimentally verified. As the implementation is focused on quantum mechanical approximations, the Numerov wavefunctions of the PI will be used for comparison as far as possible. If necessary, the PI also includes a semi-classical implementation of radial wavefunctions. The following discussion will focus on differences between both methods which might show individual errors. It is important to note that radial probability densities are compared, which however correlate directly with the radial wavefunctions.

The first state to be discussed is the ground state  $5s50s^1S_0$  which is plotted in figure 6.1. For this state the quantum defects are given with high accuracy (see table 4.1) and also

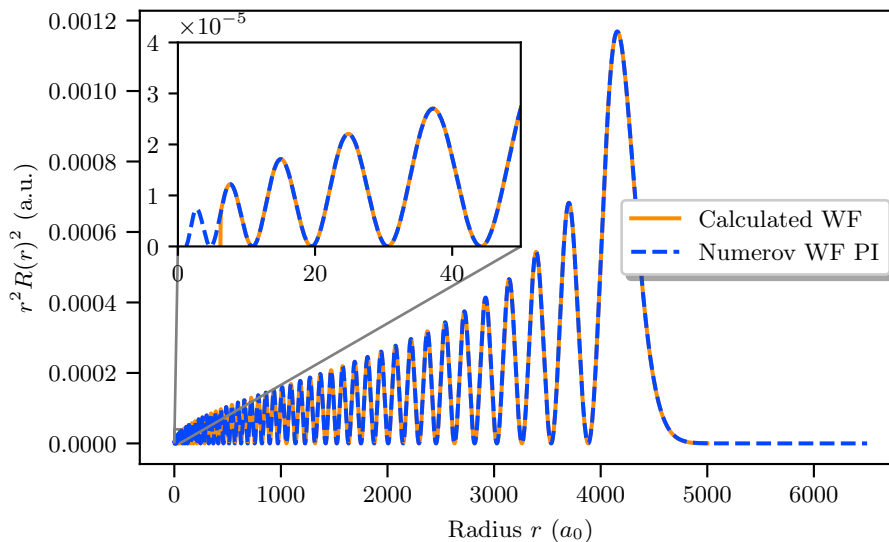


Figure 6.1.: Plot of the radial probability density  $r^2 R(r)^2$  of the Rydberg state  $5s50s^1S_0$  where  $R(r)$  denotes the radial wavefunction. For comparison the **calculated wavefunctions** are plotted with **wavefunctions calculated using the PI** [27]. The inset shows a zoomed in view of the area around the inner turning point.

show very low deviations from reference values (see table 4.2). The calculated wavefunction should therefore be as accurate as the approximation allows. As can be seen in the plot, the

calculated wavefunction shows a high level of agreement with the PI wavefunction. At very low radii the calculated wavefunction is cut off at a larger value than the PI wavefunction. This is not an error and only occurs because of technical settings. However attention has to be paid also to the inner turning point since the wavefunction integral influences the dipole matrix elements. For the Rydberg wavefunctions, the cut-off does not play a large role since the function is small for small  $r$ . Besides this effect no deviations, like phase-shifts can be observed.

The same good agreement can be found for the  $5s50p^1P_1$  state. To check if the matching between the calculated values and the PI reference is independent from the spin-series, the state  $5s50s^3S_1$  is plotted in figure 6.2. The wavefunctions again show no obvious deviations

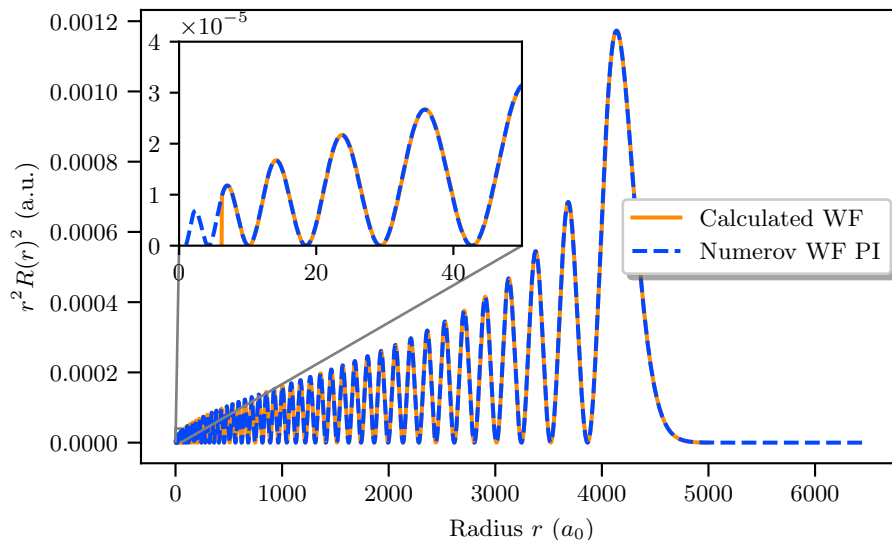


Figure 6.2.: Plot of the radial probability density  $r^2 R(r)^2$  of the Rydberg state  $5s50s^3S_1$ . Further details are given in the caption of figure 6.1.

besides the cut-off effect. This does also apply to the  $5s50p^3P_J$  states. In general the  $S$ - and  $P$ -states show a very high accordance in the Rydberg regime like it can also be seen in the quantum defects. It is expected that also the dipole matrix elements of the  $S \rightarrow P$  transitions are well in agreement with other methods.

Next to be discussed are the  $D$ -states. The calculated singlet state  $5s50d^1D_2$  wavefunction shown in figure 6.3 shows no deviations from the PI reference for large radii. At  $r \rightarrow 0$  a new effect regarding the PI wavefunction can be observed: As the inner turning point seems to be chosen too low, the wavefunctions diverge for small radii. Although this does not affect the data obtained in this work, it still has to be kept in mind that the PI reference might include errors due to divergences.

When regarding the triplet-series, another issue occurs which can already be observed in the  $5s50d^3D_1$  state wavefunction plotted in figure 6.4. A small phase-shift between the calculated wavefunction and the PI wavefunction can be observed. For  $J = 3$  this situation changes. The state  $5s50d^3D_3$  wavefunction plotted in 6.5 shows an easily visible phase-shift of approximately one  $a_0$ . As for just two methods no statement could be given about a possible flaw, it is necessary to include a third method. This is achieved by including the already mentioned semi-classical approach also implemented in the PI. Comparison of all three methods now reveals that the phase-shift presumably occurs in the implementation of this work. It can be assumed that this error occurs due to wrong quantum defect data as the  $D$ -state defects especially for the  $^3D_3$  state show some large  $n$ -dependencies (see figure 4.2).

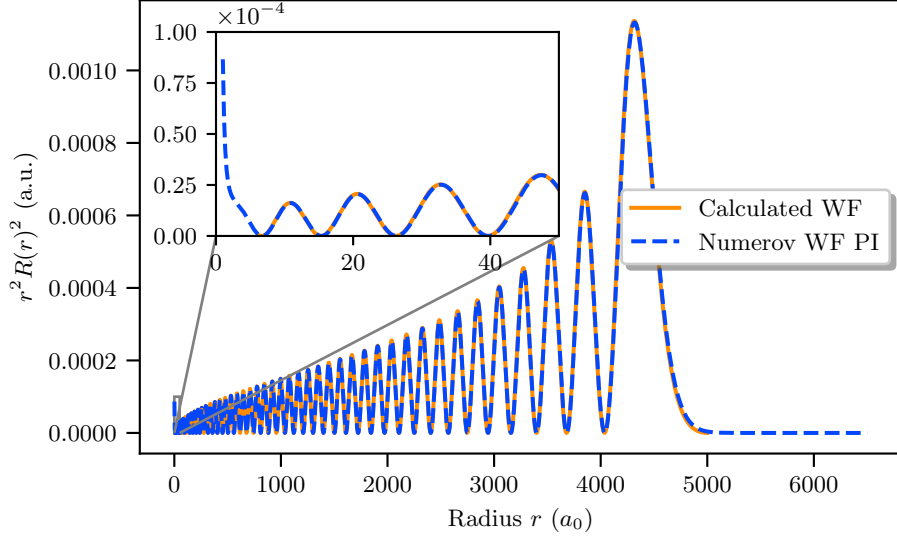


Figure 6.3.: Plot of the radial probability density  $r^2 R(r)^2$  of the Rydberg state  $5s50d^1D_2$ . Further details are given in the caption of figure 6.1.

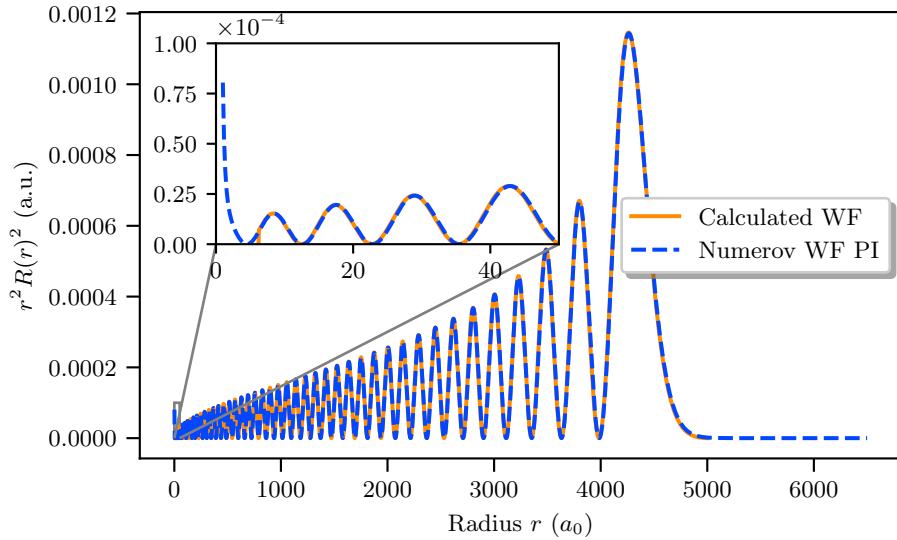


Figure 6.4.: Plot of the radial probability density  $r^2 R(r)^2$  of the Rydberg state  $5s50d^3D_1$ . Further details are given in the caption of figure 6.1.

Issues with phase-shift occurrences continue for the  $F$ -states. Here, the problem is not limited to the triplet-series but also occurs for the singlet-state  $5s50f^1F_3$ . As all  $F$ -states show approximately the same behavior, only the  $5s50f^3F_4$  state wavefunction plotted in figure 6.6 will be discussed as an example. The shift seems to be approximately two  $a_0$  and is shifted to larger radii unlike the  $D$  state in figure 6.5, where the calculated data is shifted to smaller radii compared to the PI wavefunction. For the  $F$ -state nearly no quantum defect is present and existing data largely varies for  $n \geq 25$  (see figure 4.2). This is very similar to the  $D$ -states and might lead to serious problems regarding dipole matrix element calculations. A compensation of this error could in general be accomplished by using other quantum defect data which in the best case has no deviation to the one used in reference values. This is not as simple as it might seem, since no “right” quantum defects exist. It would be necessary to

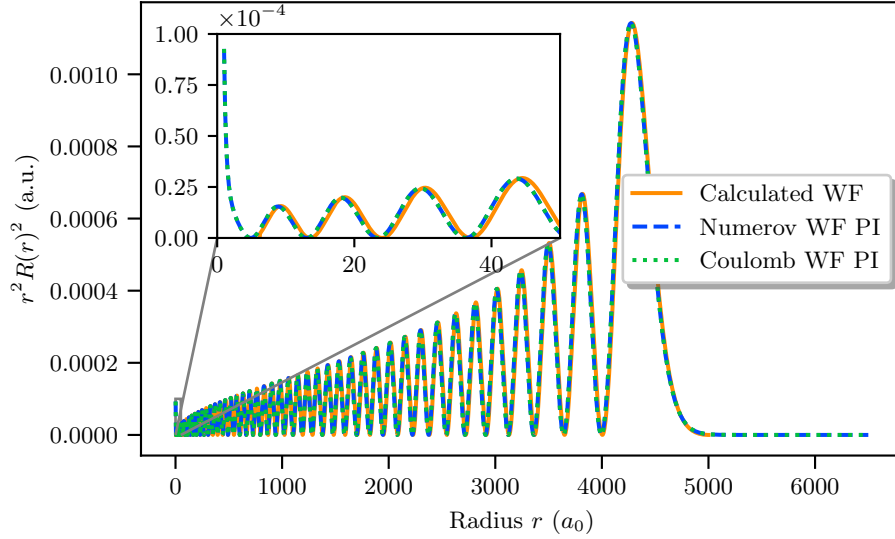


Figure 6.5.: Plot of the radial probability density  $r^2 R(r)^2$  of the Rydberg state  $5s50d^3D_3$ . For comparison the **calculated wavefunctions** are plotted with **Numerov wavefunctions** calculated using the PI and **semi-classical Coulomb functions** calculated using the PI [27].

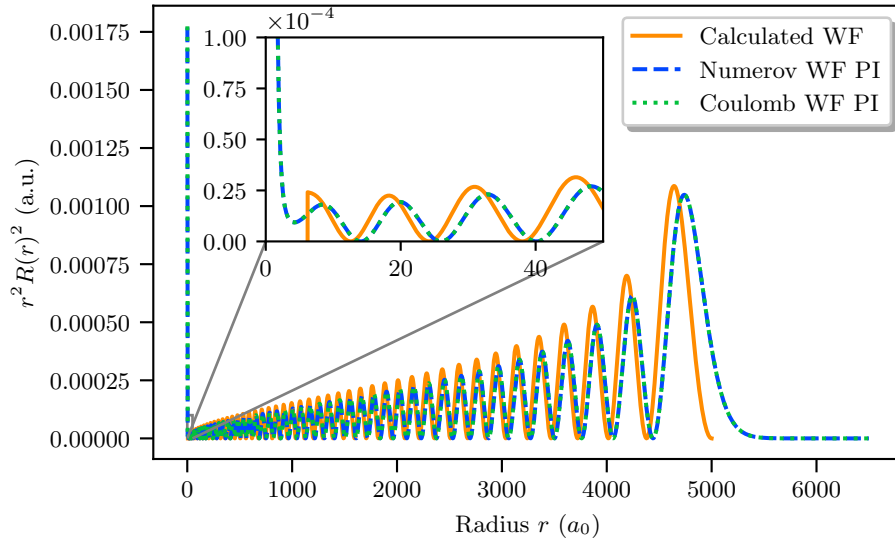


Figure 6.6.: Plot of the radial probability density  $r^2 R(r)^2$  of the Rydberg state  $5s50f^3F_3$ . Further details are given in figure 6.5.

compare the quantum defect database with many other databases and in the best case also with measured data for Rydberg states. This data is not available at the time of this work but the error has to be checked when data is available.

Currently it only seems likely that  $S$ - and  $P$ -states are calculable without large deviations. As long as no good compensation for the deviations in the  $D$ - and  $F$ -states is available, they have to be treated with care. However it is inevitable to systematically eliminate the occurring issues before future usage.

## Dipole Matrix Elements

The dipole matrix elements are calculated via the radial wavefunctions. To include angular dependencies it is necessary to calculate resulting dipole matrix elements to crosscheck the implementations of selection rules and Wigner symbols.

For comparison it is again possible to use the “Pairinteraction” Rydberg calculator (PI) v0.9.4-alpha [27] for calculating dipole matrix elements. Additionally a semi-classical approach implemented in the Alkali Rydberg Calculator (ARC) v3.0.4 [28] is used.

To allow a good graphical evaluation of the dipole matrix elements, transitions between a fixed initial state and a dynamic final state with varying principal quantum number are simulated. This also allows to identify defective principal quantum number ranges of individual methods. It is also important to discuss the obtained dipole matrix elements regarding all possible quantities which influence the results. Therefore the plotted values will be discussed regarding different transitions in general, different spin-series (singlet and triplet) and change of the initial state principal quantum number.

### General Observations

A first approach to test the obtained results is to look at example transitions between all possible angular momentum quantum numbers. That means discussing one  $S \rightarrow P$ , one  $P \rightarrow D$  and one  $D \rightarrow F$  transition. For this purpose the singlet-transitions are used.

The first transition in this comparison is the  $5s20s^1S_0$  to  $5snp^1P_1$  transition. The dipole moment is plotted in figure 6.7. As the quantum defect data for these states is given to

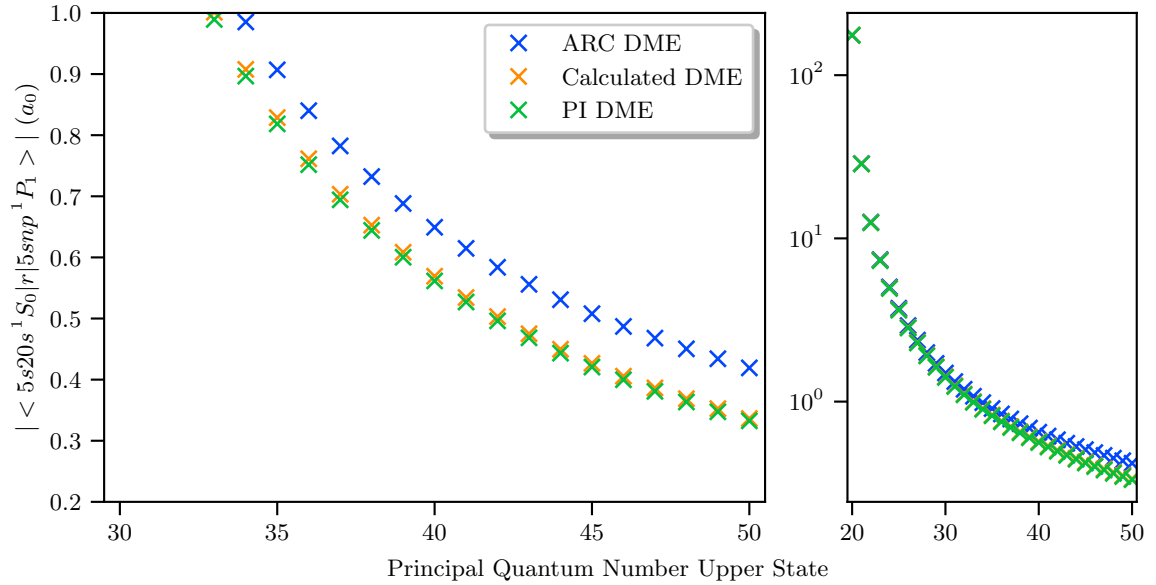


Figure 6.7.: Plots of the dipole matrix element between the states  $5s20s^1S_0$  and  $5snp^1P_1$  over the principal quantum number  $n$  of the second state. Here the  $\pi$ -transition from  $m_{J_1} = 0 \rightarrow m_{J_2} = 0$  is shown. For the discussion of the values **calculated dipole matrix elements** are compared with **dipole matrix elements calculated with the ARC** [28] and **dipole matrix elements calculated with the PI** [27].

On the left side an inset is shown to display deviations. The right side shows the whole range on a logarithmic scale.

a good accuracy (see table 4.1) and also has a low deviation to reference values (see table

4.2), it is expected that the calculated dipole matrix elements are also accurate. As can be seen in the plot, the calculated values nearly match with the reference values of the PI. The ARC matrix elements on the other hand are significantly larger than the obtained values, especially for high target- $n$ . To see the deviation more detailed, the quotient of the calculated values and the references is plotted in figure 6.8a. One can see that the quotient

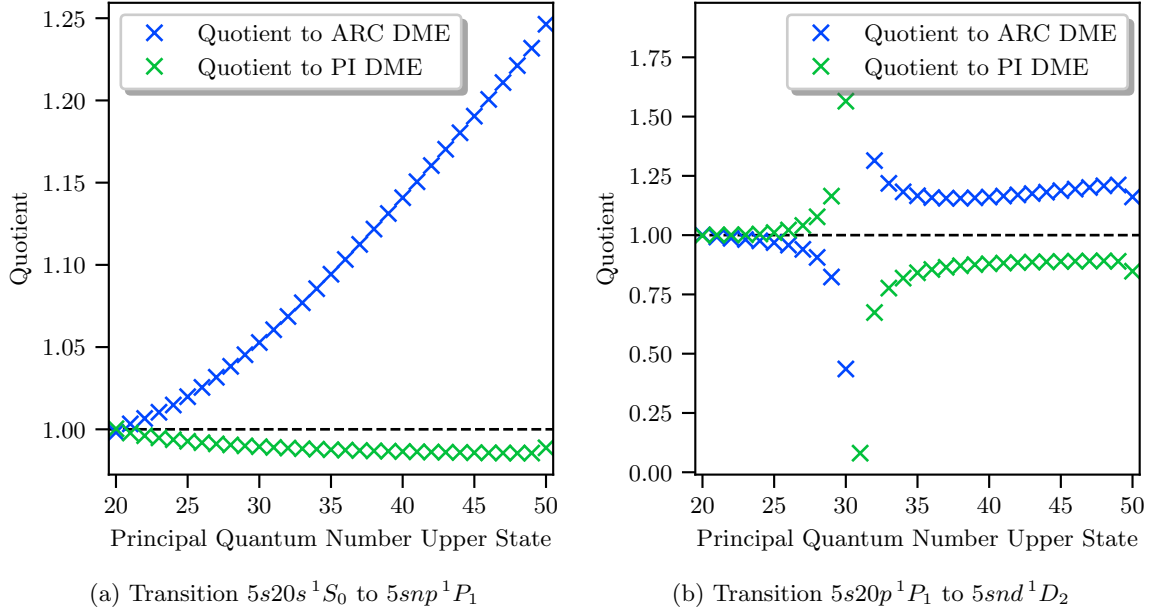


Figure 6.8.: Plot of the quotients between the calculated values and the ARC values and respectively between the calculated values and the PI values. The transition is given in the sub-caption and more detail is given in the text.

between the calculated values and the ARC values increases for larger  $n$ . This is surprising as the semi-classical approach should approach the quantum-mechanical method for Rydberg states. The PI values have a nearly constant deviation of approximately 2.5% to the calculated values. Here it would be interesting in the future, where experimental values are located.

For the second transition the states  $5s20p^1P_1$  and  $5snd^1D_2$  are observed. As the final state is a  $D$ -state, it can be expected that errors occur since a large  $n$  dependency can be seen in figure 4.2. This indicates a large interaction with the ground state valence electron which can lead to errors due to the used approximations. In figure 6.9 the obtained data out of all three methods is shown. The data seems to vary between all three methods. To observe tendencies especially of the Coulomb approximation the quotient between the methods is plotted in figure 6.8b. The quotients show a large resonance located at the zero point of the dipole matrix element. This is related to the fact, that the matrix elements get very small at this point but still have a constant absolute deviation. Therefore the relative deviation, calculated via the quotient, diverges. The resonance location at target- $n$  values of approximately 30 has its source in the wavefunctions, as minima and maxima of the functions cancel each other out in this region. A shift of the wavefunctions can be excluded by plotting the wavefunctions of initial and final state.

Besides this effect it is hard to derive statements about the accuracy of the method from this transition. Even though the deviation from the PI values is smaller than the one from the ARC values it is still in the region of about 10% to 15% which is large compared to the results obtained from the  $S \rightarrow P$  transition. This could introduce large errors in stark map calculations.

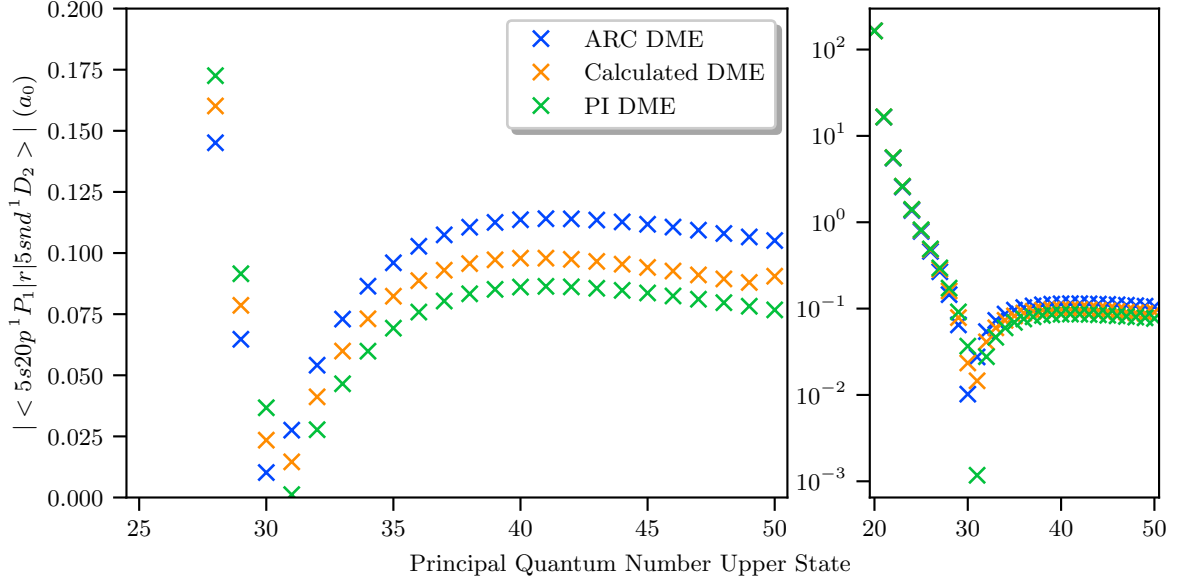


Figure 6.9.: Plots of the dipole matrix element between the states  $5s20p^1P_1$  and  $5snd^1D_2$  over the principal quantum number  $n$  of the second state. Here the  $\pi$ -transition from  $m_{J_1} = 1 \rightarrow m_{J_2} = 1$  is shown. Detail on the colors and the subplots is given in the caption of figure 6.7.

The third transition to be discussed is the transition between  $5s20d^1D_2$  and  $5snf^1F_3$ . The results are shown in figure 6.10. Although the initial state is a  $D$ -state no large deviations

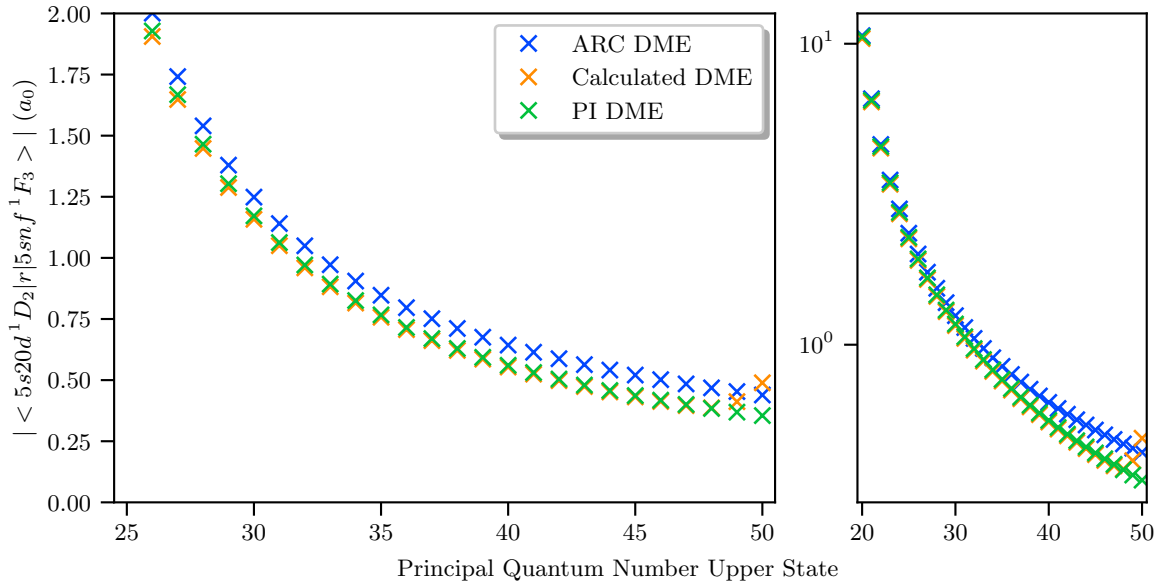


Figure 6.10.: Plots of the dipole matrix element between the states  $5s20d^1D_2$  and  $5snf^1F_3$  over the principal quantum number  $n$  of the second state. Here the  $\pi$ -transition from  $m_{J_1} = 2 \rightarrow m_{J_2} = 2$  is shown. Detail on the colors and the subplots is given in the caption of figure 6.7.

to the PI values can be observed. Only for large  $n$  the calculated values seem to diverge. However, the transition probabilities are small in that regime and are therefore negligible.

By calculating the dipole matrix elements up to  $n = 55$  it can be shown, that the increase of the matrix elements is only a local maximum. As this does not occur in the other methods, there must be an error in the Coulomb approximation. This might have its source in numerical errors due to turning points or divergences of the wavefunction. When examining the wavefunctions of those states no obvious errors can be observed. However this occurrence has to be double-checked with other  $D \rightarrow F$  transitions to evaluate its severity.

### Singlet- and Triplet-Series

As the singlet- and triplet-series are treated separately, it is also necessary to take a look at the dipole matrix elements when the spin of the states is changed.

The transition between the states  $5s20s^3S_1$  and  $5snp^3P_1$  plotted in figure 6.11 validates the observations of figure 6.7. The calculated values seem to match the PI values. The ARC

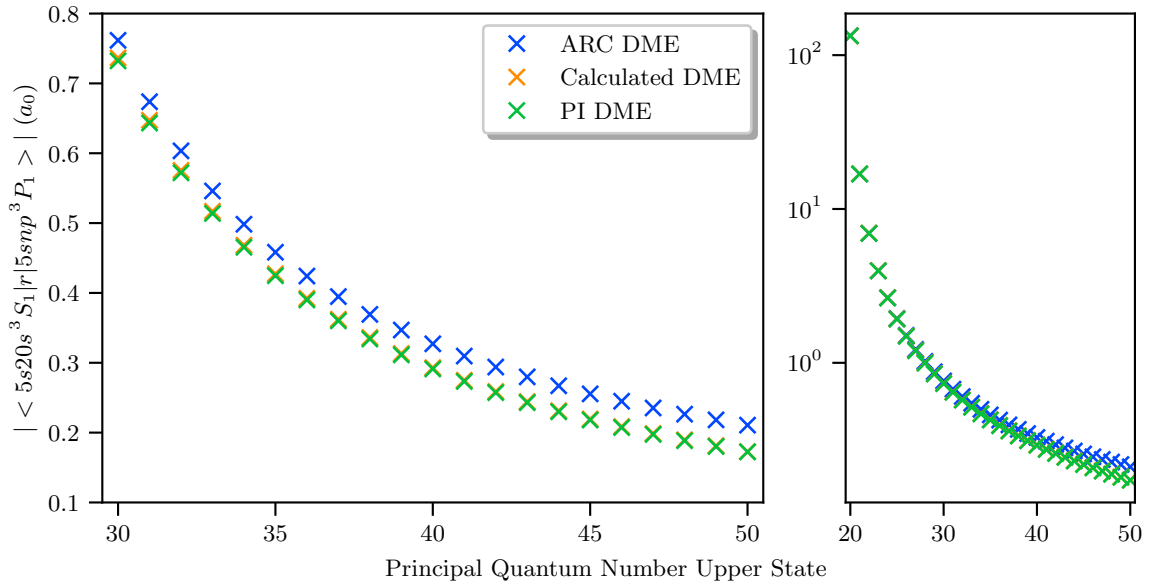


Figure 6.11.: Plots of the dipole matrix element between the states  $5s20s^3S_1$  and  $5snp^3P_1$  over the principal quantum number  $n$  of the second state. Here the  $\pi$ -transition from  $m_{J_1} = 1 \rightarrow m_{J_2} = 1$  is shown. Detail on the colors and the subplots is given in the caption of figure 6.7.

matrix elements are again larger than the other two approximations. This is the same behavior as for the singlet  $S \rightarrow P$  transition.

As the  $D$ -states have shown severe deviations in the singlet-series, it is probable that similar problems occur for the triplet-series. This is indeed the case for the  $5s20d^3D_3$  to  $5snf^3F_3$  transition as seen in picture 6.12. The increasing dipole matrix element at  $n \rightarrow 50$  still exists and furthermore the values show a large deviation from both other methods.

In the case of the  $5s20p^3P_2$  to  $5snd^3D_2$  transition shown in figure 6.13, the tendency for large principal quantum numbers looks promising. The deviation to the PI values vanishes as for the  $S \rightarrow P$  transitions. However for small target- $n$  large deviations occur as the calculated matrix elements decrease faster as the other two methods predict. Errors like this can always result from finite accuracy of the quantum defects. By varying the starting state to a higher principal quantum number, possible errors, created by the strong  $n$ -dependence for low- $n$  quantum defects, could be circumvented.

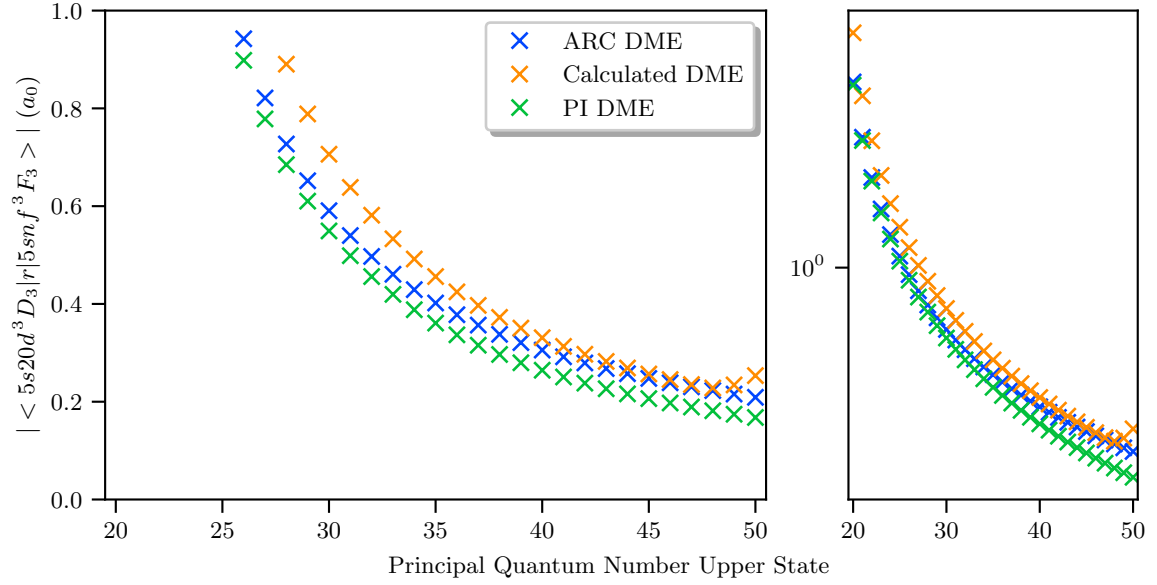


Figure 6.12.: Plots of the dipole matrix element between the states  $5s20d^3D_3$  and  $5snf^3F_3$  over the principal quantum number  $n$  of the second state. Here the  $\pi$ -transition from  $m_{J_1} = 3 \rightarrow m_{J_2} = 3$  is shown. Detail on the colors and the subplots is given in the caption of figure 6.7.

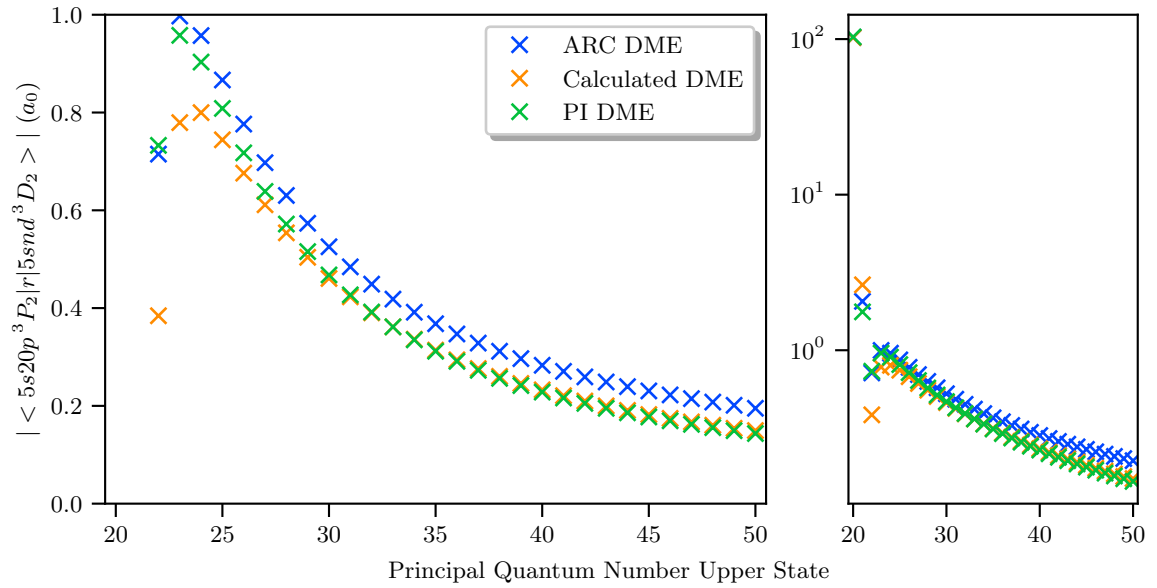


Figure 6.13.: Plots of the dipole matrix element between the states  $5s20p^3P_2$  and  $5snd^3D_2$  over the principal quantum number  $n$  of the second state. Here the  $\pi$ -transition from  $m_{J_1} = 2 \rightarrow m_{J_2} = 2$  is shown. Detail on the colors and the subplots is given in the caption of figure 6.7.

### Change of Initial State

As some tendencies were already outlined before, only the critical transitions should be discussed in details regarding a change of the initial state. By changing the principal quantum number of the initial state it is expected that errors induced by the quantum defect data disappear or at least change. Disappearing errors can be a sign for a principal quantum

number for Rydberg state treatment, which is chosen too low.

The  $S \rightarrow P$  transitions show the same behavior as in the two cases considered before. This was checked with the  $5s30s^1S_0$  to  $5snp^1P_1$  and the  $5s30s^3S_1$  to  $5snp^3P_1$  transitions. As no new effects were observed, these transitions should not be discussed further.

Transitions including  $D$ -states again show problematic behavior. This is mainly the case for the  $5s30p^1P_1$  to  $5snd^1D_2$  transition shown in figure 6.14 and the  $5s30d^3D_3$  to  $5snf^3F_3$  shown in figure 6.15. These two transitions did already show discrepancies for a principal

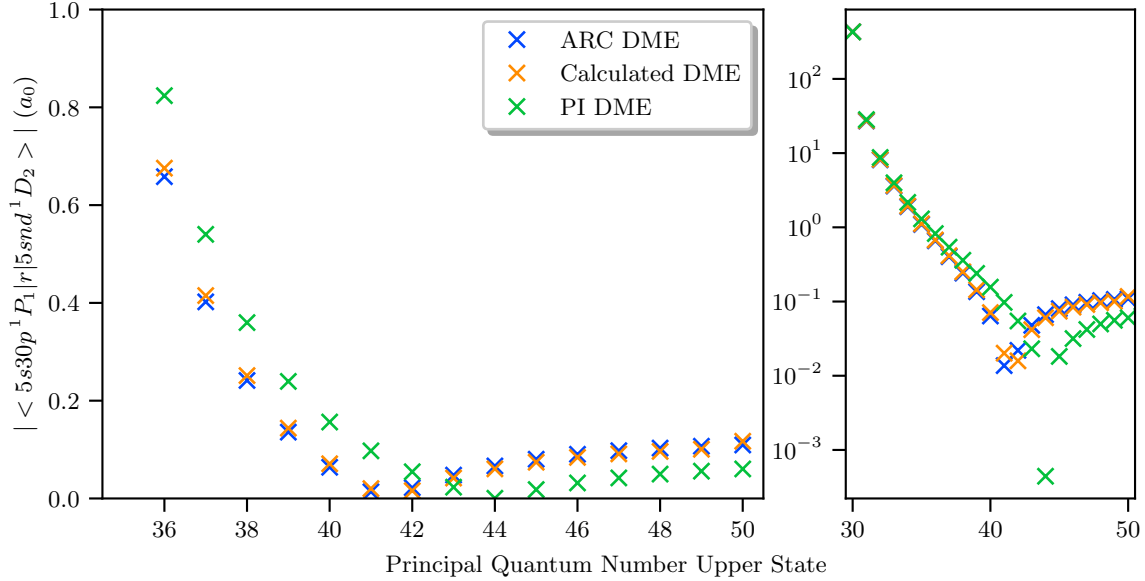


Figure 6.14.: Plots of the dipole matrix element between the states  $5s30p^1P_1$  and  $5snd^1D_2$  over the principal quantum number  $n$  of the second state. Here the  $\pi$ -transition from  $m_{J_1} = 1 \rightarrow m_{J_2} = 1$  is shown. Detail on the colors and the subplots is given in the caption of figure 6.7.

quantum number of  $n = 20$  of the first state (see figure 6.9 and 6.12). For the higher  $n$  of the initial state the error seems to change. In the case of the first transition it now appears as if the ARC data and the calculated values match over nearly the whole range. Without detailed analysis of the PI calculation no obvious outline about this transition can be given. The second transition from  $5s30d^3D_3$  to  $5snf^3F_3$  has a smaller deviation between the methods than the  $5s20d^3D_3$  to  $5snf^3F_3$  transition shown in figure 6.12. It can be concluded, that indeed most of the deviations between the three implementations are caused by the lower state as it was expected since the approximation mostly affects low- $n$  states.

The transitions  $5s20d^1D_2$  to  $5snf^1F_3$  and  $5s20p^3P_2$  to  $5snd^3D_2$  shown in figure 6.16 and 6.17 do look more promising regarding at least high quantum numbers. This confirms the observations made regarding figure 6.10 and 6.13. The errors which occurred for a lower initial state decrease and the calculated data seems to converge with the PI reference for large  $n$ . It is still possible to observe an increase of the matrix element in figure 6.16 but this appears to be a local problem in this regime.

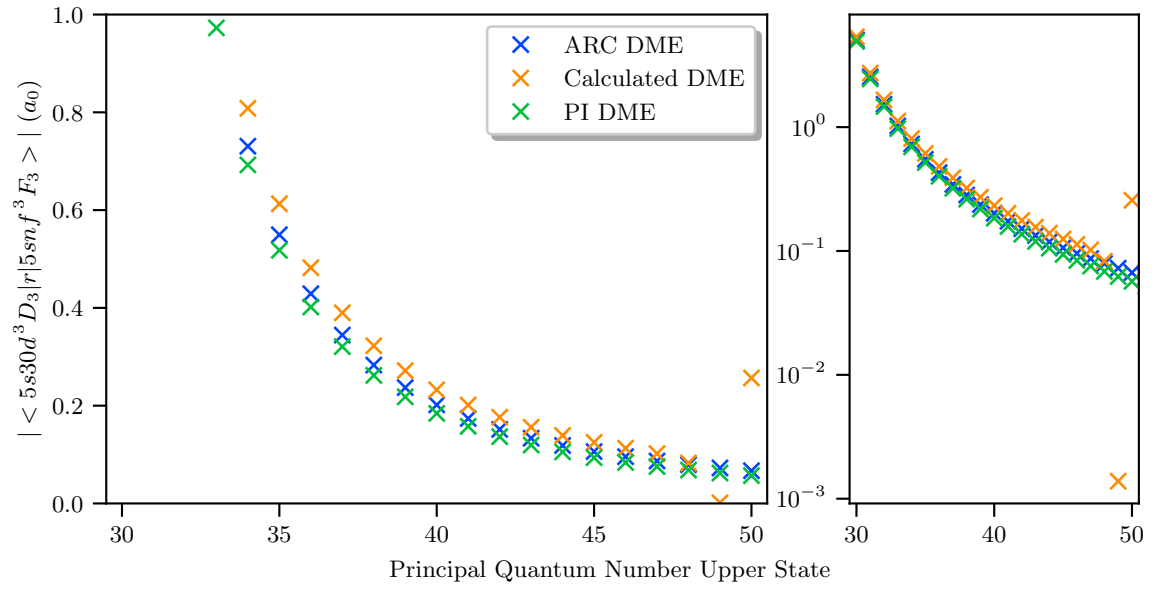


Figure 6.15.: Plots of the dipole matrix element between the states  $5s30d^3D_3$  and  $5snf^3F_3$  over the principal quantum number  $n$  of the second state. Here the  $\pi$ -transition from  $m_{J_1} = 3 \rightarrow m_{J_2} = 3$  is shown. Detail on the colors and the subplots is given in the caption of figure 6.7.

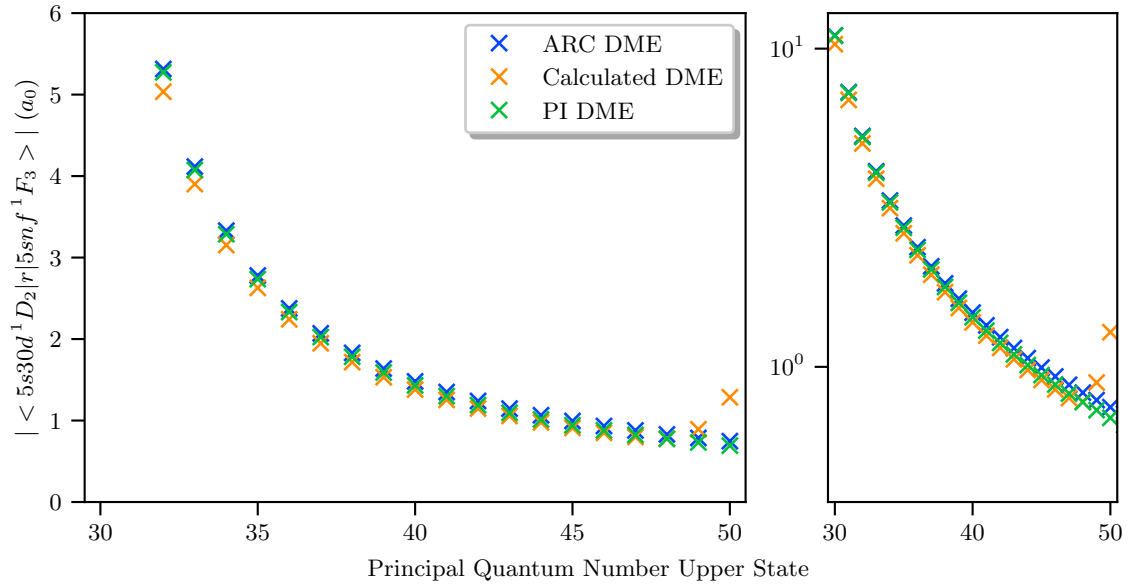


Figure 6.16.: Plots of the dipole matrix element between the states  $5s20d^1D_2$  and  $5snf^1F_3$  over the principal quantum number  $n$  of the second state. Here the  $\pi$ -transition from  $m_{J_1} = 2 \rightarrow m_{J_2} = 2$  is shown. Detail on the colors and the subplots is given in the caption of figure 6.7.

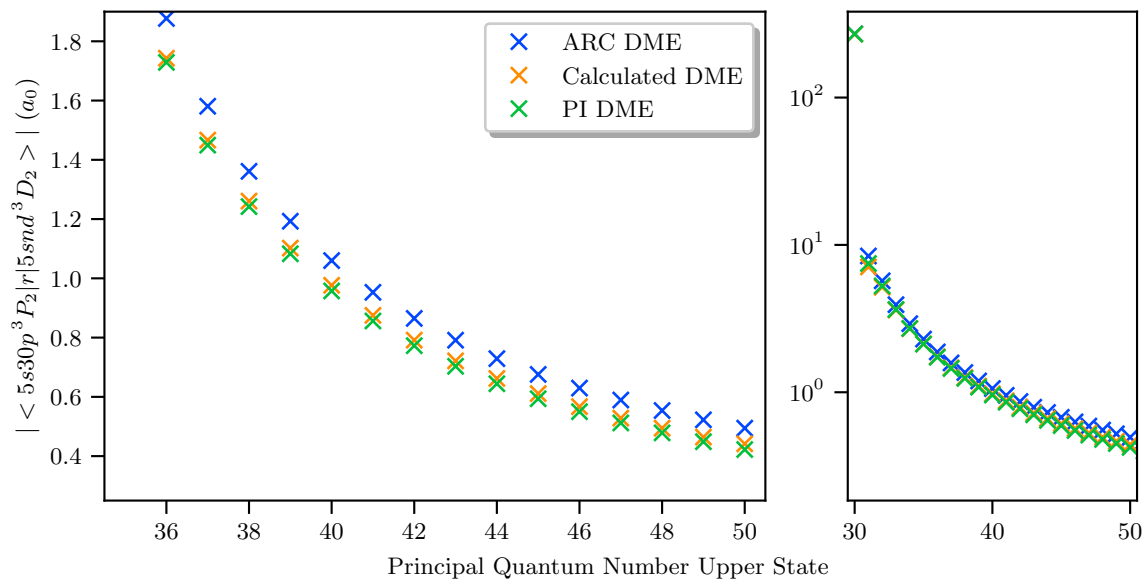


Figure 6.17.: Plots of the dipole matrix element between the states  $5s20p^3P_2$  and  $5snd^3D_2$  over the principal quantum number  $n$  of the second state. Here the  $\pi$ -transition from  $m_{J_1} = 2 \rightarrow m_{J_2} = 2$  is shown. Detail on the colors and the subplots is given in the caption of figure 6.7.

## 7. Summary and Outlook

The goal of this work was to calculate wavefunctions and dipole matrix elements of the alkaline-earth atom  $^{88}\text{Sr}$ . For this purpose, a theoretical foundation consisting of quantum-mechanical principles and calculation methods was introduced.

Atomic potentials were discussed regarding the importance of potential terms in different radial regimes. Furthermore it was outlined, why a simplified potential approach is sufficient for treating Rydberg states when combined with experimental quantum defect data.

The physical properties of the quantum defect were discussed and a database was calculated. As a final approach the Coulomb approximation was proposed and discussed. A detailed outline about the influence of the quantum defects in the approximation was given. A documented numerical implementation of the Coulomb equation, obtained by the approximation, was done and limitations were discussed.

By comparing the obtained results with two other readily available implementations, the results were set in context. It was observed, that calculations of the  $S$ -states and  $P$ -states with  $n \geq 20$  agree very well across all used methods. Neither the wavefunctions nor the dipole matrix elements showed large deviations. Transitions including  $D$ -states have shown large deviation. The wavefunction calculation for the singlet-series was constant across the implementations, but phase-shifts occurred for the triplet-series when using  $J \geq 2$ . This error led to the dipole matrix elements to also differ between the methods. The discussed transitions to an  $^3D_2$  state gave quite good results for higher states, where surprisingly transitions to an  $^1D_2$  state gave deviating results even for high Rydberg states. The  $F$ -state wavefunctions showed large phase-shifts when compared to reference values. This error is expected to have its source in the quantum defect data which would confirm the observation, that at least singlet transitions gave comparable results for high principal quantum numbers. Transitions to triplet-series deviated also for high initial states.

In conclusion it can be said, that a good accordance with reference methods was achieved in most of the cases. Deviations occurring between the approximations can partly be traced back to the quantum defect data, but no general claim can be made, why certain deviations occur. Just by regarding the comparison with the reference methods, the approach does work good for Rydberg state calculations. Limitations occur when calculating high- $L$  states. It will be necessary in the future to include experimental reference values to eliminate errors due to the approximation.

The implementation of Rydberg state calculations gives an important foundation for our quantum simulator setup using circular Rydberg states [15]. Discussions of the results did show difficulties when calculating high- $L$  states. This remains a challenge for the future, that can be solved by implementing hydrogen wavefunctions, as core defects get negligible for high- $L$  states.

With the obtained dipole matrix elements it will be possible to calculate stark maps. This step is mathematically difficult as large hamiltonians need to be diagonalized. Calculated stark maps for strontium could then be compared with the work of Millen et al. [55] which is currently (to the authors knowledge) the only source for literature values of stark maps. This comparison here is very important as for example stark maps calculated with the alkali Rydberg calculator [28] show large deviations to those experimental values. If accurate stark maps are obtained they allow for example high precision calculations of avoided cross-

ings needed for the circularization method of Delande et al. [56] is used. This method uses ramped crossed electric and magnetic fields which has to be precise to have full control over the transitions. For this method it is also required that the stark map calculation code supports arbitrary angles between the electric and magnetic field, which is not supported by any publicly available implementation.

With a working implementation of all calculations outlined in this section it will finally be possible to supply the quantum simulator experiment and also further experiments with accurate atomic state data for all purposes.

# A. Appendix

## A.1. Quantum Defects of Strontium

In the following tables [A.2](#), [A.3](#) and [A.4](#) the known quantum defects of strontium are listed. The collection includes values from different experiment papers published up to the date of this thesis. The quantum defects are either obtained by experiment or calculated. Since each paper only considers a limited  $n$ -range, it is not possible to find quantum defects for every principal quantum number. Where alternative data points were available, the one with the best accuracy was chosen. The sources for every value are listed in table [A.1](#).

Table A.1.: Overview of all sources used in table [A.2](#), [A.3](#) and [A.4](#) sorted by state and  $n$ -range.

	State	$n$ -range	Source
$L = 0$	$5sns^1S_0$	5 to 9	Rubbmark et al., PS 18, 196 (1978) <a href="#">[51]</a>
		10 to 80	Beigang et al., OC 42, 19 (1982) <a href="#">[57]</a>
	$5sns^3S_1$	11 to 45	Beigang et al., PS 26, 183 (1982) <a href="#">[58]</a>
$L = 1$	$5snp^1P_1$	5 to 29	Rubbmark et al., PS 18, 196 (1978) <a href="#">[51]</a>
	$5snp^3P_2$	5 to 60	Armstrong et al., JOSA 69, 211 (1979) <a href="#">[59]</a>
	$5snp^3P_1$	5 to 22	Armstrong et al., JOSA 69, 211 (1979) <a href="#">[59]</a>
	$5snp^3P_0$	5 to 15	Armstrong et al., JOSA 69, 211 (1979) <a href="#">[59]</a>
$L = 2$	$5snd^1D_2$	4 to 9	Rubbmark et al., PS 18, 196 (1978) <a href="#">[51]</a>
		10 to 80	Beigang et al., OC 42, 19 (1982) <a href="#">[57]</a>
	$5snd^3D_3$	4 to 8	Rubbmark et al., PS 18, 196 (1978) <a href="#">[51]</a>
		12 to 45	Beigang et al., PS 26, 183 (1982) <a href="#">[58]</a>
$5snd^3D_2$	4 6 to 50	Rubbmark et al., PS 18, 196 (1978) <a href="#">[51]</a> Esherick, PRA 15, 1920 (1977) <a href="#">[60]</a>	
$5snd^3D_1$	4 to 7 12 to 32	Rubbmark et al., PS 18, 196 (1978) <a href="#">[51]</a> Beigang et al., PS 26, 183 (1982) <a href="#">[58]</a>	
$L = 3$	$5snf^1F_3$	4 to 29	Rubbmark et al., PS 18, 196 (1978) <a href="#">[51]</a>
	$5snf^3F_4$	4 to 28	Rubbmark et al., PS 18, 196 (1978) <a href="#">[51]</a>
	$5snf^3F_3$	4 to 28	Rubbmark et al., PS 18, 196 (1978) <a href="#">[51]</a>
	$5snf^3F_2$	4 to 28	Rubbmark et al., PS 18, 196 (1978) <a href="#">[51]</a>

Table A.2.: Quantum defects of the strontium  $5sns^1S_0$ ,  $5snp^1P_1$ ,  $5snd^1D_2$ ,  $5snf^1F_3$ ,  $5sns^3S_1$ ,  $5snp^3P_2$  and  $5snp^3P_1$  states in the  $n$ -range from 4 to 40. The source for every quantum defect is listed in table A.1.

n	$5sns^1S_0$	$5snp^1P_1$	$5snd^1D_2$	$5snf^1F_3$	$5sns^3S_1$	$5snp^3P_2$	$5snp^3P_1$
4			1.936929	-0.143061			
5	3.4543267	2.8720247	1.870486	0.013466		3.120	3.131
6	3.325401	2.954799	1.792596	0.04308		2.971	2.984
7	3.1718327	3.047734	1.82690	0.05611		2.883	2.893
8	3.25784	2.37624	1.86021	0.06352		2.886	2.896
9	3.26419	2.50856	1.89910	0.06836		2.883	2.893
10	3.26612	2.58484	1.94844	0.07186		2.880	2.890
11	3.26699	2.62804	1.99580	0.07406	3.3780	2.888	2.888
12	3.26846	2.65408	2.02346	0.0759	3.3770	2.877	2.887
13	3.26754	2.67109	2.07954	0.0772	3.3749	2.876	2.886
14	3.26782	2.6828	2.13058	0.0781	3.3745	2.875	2.885
15	3.26801	2.6908	2.18851	0.0792	3.3734	2.875	2.885
16	3.26815	2.6968	2.12569	0.0799	3.3736	2.875	2.885
17	3.26826	2.7017	2.16944	0.0802	3.3726	2.874	2.884
18	3.26834	2.7051	2.19997	0.0809	3.3730	2.874	2.885
19	3.26842	2.7082	2.22417	0.0814	3.3727	2.874	2.884
20	3.26848	2.7100	2.24283	0.0811	3.373	2.875	2.884
21	3.26853	2.7120	2.25809	0.0816	3.371	2.874	2.884
22	3.26857	2.7127	2.27090	0.0821	3.374	2.875	2.885
23	3.26860	2.7140	2.28184	0.082	3.376	2.876	
24	3.26863	2.7156	2.29129	0.082	3.373	2.876	
25		2.717	2.29952	0.080	3.366	2.878	
26	3.26869	2.716	2.30675	0.087	3.364	2.877	
27		2.716		0.068	3.370	2.878	
28	3.26872	2.716	2.31876	0.081	3.369	2.876	
29		2.725	2.32380	0.064	3.372	2.874	
30	3.26876		2.32831		3.375	2.880	
31			2.33236		3.374	2.876	
32	3.26878		2.33601		3.381	2.874	
33			2.33932		3.354	2.875	
34	3.26880		2.34232		3.366	2.876	
35			2.34505		3.359	2.879	
36	3.26882		2.34755		3.370	2.878	
37	3.26883		2.34984		3.373	2.879	
38	3.26883		2.35193		3.371	2.879	
39	3.26884		2.35386		3.37	2.885	
40	3.26884		2.35564		3.37	2.877	

Table A.3.: Continuation of table A.2 for the  $n$ -range from 41 to 80. The source for every quantum defect is also listed in table A.1.

n	$5sns^1S_0$	$5snp^1P_1$	$5snd^1D_2$	$5snf^1F_3$	$5sns^3S_1$	$5snp^3P_2$	$5snp^3P_1$
41	3.26885				3.36	2.878	
42	3.26885		2.35881		3.37	2.865	
43	3.26886		2.36022		3.33	2.872	
44	3.26886		2.36154		3.36	2.887	
45	3.26887		2.36276		3.39	2.892	
46	3.26887		2.36390			2.894	
47	3.26887		2.36496			2.898	
48	3.26888		2.36596			2.888	
49	3.26888		2.36689			2.894	
50	3.26888		2.36777			2.885	
51	3.26888		2.36859			2.870	
52	3.26889		2.36936			2.878	
53	3.26889		2.37009			2.919	
54	3.26889		2.37078			2.887	
55	3.26889		2.37143			2.872	
56	3.26890		2.37204			2.889	
57	3.26890		2.37262			2.897	
58	3.26890		2.37317			2.924	
59	3.26890		2.37369			2.916	
60	3.26890		2.37418			2.922	
61	3.26890		2.37465				
62	3.26890		2.37509				
63	3.26891		2.37551				
64	3.26891		2.37592				
65	3.26891		2.37630				
66	3.26891		2.37667				
67	3.26891		2.37702				
68	3.26891		2.37735				
69	3.26891		2.37767				
70	3.26891		2.37797				
71							
72							
73							
74			2.37906				
75	3.26892		2.37931				
76							
77							
78							
79			2.38019				
80	3.26892		2.38039				

Table A.4.: Quantum defects of the strontium  $5snp^3P_0$ ,  $5snd^3D_3$ ,  $5snd^3D_2$ ,  $5snd^3D_1$ ,  $5snf^3F_4$ ,  $5snf^3F_3$  and  $5snf^3F_2$  states in the  $n$ -range from 4 to 50. The source for every quantum defect is listed in table A.1.

n	$5snp^3P_0$	$5snd^3D_3$	$5snd^3D_2$	$5snd^3D_1$	$5snf^3F_4$	$5snf^3F_3$	$5snf^3F_2$
4		2.0064805	2.0100976	2.0122392	0.089724	0.090475	0.091018
5	3.137	1.8251699		1.8307130	0.097292	0.097922	0.09840
6	2.986	1.802713	1.807	1.808522	0.101407	0.10195	0.10244
7	2.898	1.799302	1.804	1.806028	0.10379	0.10443	0.10489
8	2.901	1.80282	1.808		0.10546	0.10620	0.10665
9	2.897		1.817		0.10658	0.10726	0.10770
10	2.895		1.832		0.10756	0.10831	0.10831
11	2.893		1.853		0.10783	0.10872	0.10872
12	2.891	1.8586	1.884	1.9114	0.1082	0.1090	0.1090
13	2.891	1.8860	1.929	1.9801	0.1084	0.1092	0.1092
14	2.890	1.9181	1.990	2.0821	0.1095	0.1095	0.1095
15	2.890	1.9632	2.063	2.2151	0.1103	0.1103	0.1103
16		2.0194	2.127	2.3717	0.1101	0.1101	0.1101
17		2.0824	2.351	2.4418	0.1106	0.1106	0.1106
18		2.1567	2.424	2.5014	0.1100	0.1100	0.1100
19		2.225	2.478	2.541	0.1118	0.1118	0.1118
20		2.289	2.515	2.571	0.1113	0.1113	0.1113
21		2.347	2.542	2.592	0.1119	0.1119	0.1119
22		2.366	2.562	2.606	0.1118	0.1118	0.1118
23		2.420	2.577	2.615	0.112	0.112	0.112
24		2.448	2.589	2.622	0.112	0.112	0.112
25		2.481	2.598	2.628	0.101	0.101	0.101
26		2.488	2.605	2.630	0.122	0.122	0.122
27		2.515	2.611	2.640	0.118	0.118	0.118
28		2.524	2.616	2.638	0.110	0.110	0.110
29		2.528	2.620	2.642			
30		2.546	2.624	2.651			
31		2.561	2.627	2.654			
32		2.544	2.629	2.651			
33		2.573	2.632				
34		2.579	2.634				
35		2.568	2.636				
36		2.579	2.637				
37		2.543	2.639				
38		2.57	2.640				
39		2.56	2.641				
40		2.56	2.642				
41		2.57	2.643				
42		2.54	2.644				
43		2.54	2.645				
44		2.58	2.645				
45		2.54	2.646				
46			2.647				
47			2.647				
48			2.648				
49			2.648				
50			2.649				

## 8. Bibliography

- [1] Richard P. Feynman. “Simulating physics with computers”. In: *International Journal of Theoretical Physics* 21.6-7 (1982), pp. 467–488. ISSN: 0020-7748. DOI: [10.1007/BF02650179](https://doi.org/10.1007/BF02650179) (cit. on p. 1).
- [2] Iulia Buluta and Franco Nori. “Quantum simulators”. In: *Science (New York, N.Y.)* 326.5949 (2009), pp. 108–111. DOI: [10.1126/science.1177838](https://doi.org/10.1126/science.1177838) (cit. on p. 1).
- [3] I. M. Georgescu, S. Ashhab, and Franco Nori. “Quantum simulation”. In: *Reviews of Modern Physics* 86.1 (2014), pp. 153–185. ISSN: 0034-6861. DOI: [10.1103/RevModPhys.86.153](https://doi.org/10.1103/RevModPhys.86.153) (cit. on p. 1).
- [4] S. Somaroo et al. “Quantum Simulations on a Quantum Computer”. In: *Physical Review Letters* 82.26 (1999), pp. 5381–5384. ISSN: 0031-9007. DOI: [10.1103/PhysRevLett.82.5381](https://doi.org/10.1103/PhysRevLett.82.5381) (cit. on p. 1).
- [5] Andrew A. Houck, Hakan E. Türeci, and Jens Koch. “On-chip quantum simulation with superconducting circuits”. In: *Nature Physics* 8.4 (2012), pp. 292–299. ISSN: 1745-2473. DOI: [10.1038/nphys2251](https://doi.org/10.1038/nphys2251) (cit. on p. 1).
- [6] R. Blatt and C. F. Roos. “Quantum simulations with trapped ions”. In: *Nature Physics* 8.4 (2012), pp. 277–284. ISSN: 1745-2473. DOI: [10.1038/nphys2252](https://doi.org/10.1038/nphys2252) (cit. on p. 1).
- [7] C. Kokail et al. “Self-verifying variational quantum simulation of lattice models”. In: *Nature* 569.7756 (2019), pp. 355–360. DOI: [10.1038/s41586-019-1177-4](https://doi.org/10.1038/s41586-019-1177-4) (cit. on p. 1).
- [8] Immanuel Bloch, Jean Dalibard, and Sylvain Nascimbène. “Quantum simulations with ultracold quantum gases”. In: *Nature Physics* 8.4 (2012), pp. 267–276. ISSN: 1745-2473. DOI: [10.1038/nphys2259](https://doi.org/10.1038/nphys2259) (cit. on p. 1).
- [9] Alán Aspuru-Guzik and Philip Walther. “Photonic quantum simulators”. In: *Nature Physics* 8.4 (2012), pp. 285–291. ISSN: 1745-2473. DOI: [10.1038/nphys2253](https://doi.org/10.1038/nphys2253) (cit. on p. 1).
- [10] T. Hensgens et al. “Quantum simulation of a Fermi-Hubbard model using a semiconductor quantum dot array”. In: *Nature* 548.7665 (2017), pp. 70–73. DOI: [10.1038/nature23022](https://doi.org/10.1038/nature23022) (cit. on p. 1).
- [11] Hannes Bernien et al. “Probing many-body dynamics on a 51-atom quantum simulator”. In: *Nature* 551.7682 (2017), pp. 579–584. DOI: [10.1038/nature24622](https://doi.org/10.1038/nature24622) (cit. on p. 1).
- [12] Henning Labuhn et al. “Tunable two-dimensional arrays of single Rydberg atoms for realizing quantum Ising models”. In: *Nature* 534.7609 (2016), pp. 667–670. DOI: [10.1038/nature18274](https://doi.org/10.1038/nature18274) (cit. on p. 1).
- [13] Harry Levine et al. “High-fidelity control and entanglement of Rydberg atom qubits”. In: *Physical Review Letters* 121.12 (2018). ISSN: 0031-9007. DOI: [10.1103/PhysRevLett.121.123603](https://doi.org/10.1103/PhysRevLett.121.123603). URL: <http://arxiv.org/pdf/1806.04682v1> (cit. on p. 1).
- [14] T. L. Nguyen et al. “Towards Quantum Simulation with Circular Rydberg Atoms”. In: *Physical Review X* 8.1 (2018). DOI: [10.1103/PhysRevX.8.011032](https://doi.org/10.1103/PhysRevX.8.011032) (cit. on p. 1).

- [15] Florian Meinert et al. “Indium tin oxide films meet circular Rydberg atoms: Prospects for novel quantum simulation schemes”. In: *Physical Review Research* 2.2 (2020). DOI: [10.1103/PhysRevResearch.2.023192](https://doi.org/10.1103/PhysRevResearch.2.023192) (cit. on pp. 1, 49).
- [16] D. Barredo et al. “Three-Dimensional Trapping of Individual Rydberg Atoms in Ponderomotive Bottle Beam Traps”. In: *Physical Review Letters* 124.2 (2020), p. 023201. ISSN: 0031-9007. DOI: [10.1103/PhysRevLett.124.023201](https://doi.org/10.1103/PhysRevLett.124.023201) (cit. on p. 1).
- [17] B. Darquié et al. “Controlled single-photon emission from a single trapped two-level atom”. In: *Science (New York, N.Y.)* 309.5733 (2005), pp. 454–456. DOI: [10.1126/science.1113394](https://doi.org/10.1126/science.1113394) (cit. on p. 1).
- [18] F. B. Dunning et al. “Recent advances in Rydberg physics using alkaline-earth atoms”. In: *Journal of Physics B: Atomic, Molecular and Optical Physics* 49.11 (2016), p. 112003. ISSN: 0953-4075. DOI: [10.1088/0953-4075/49/11/112003](https://doi.org/10.1088/0953-4075/49/11/112003) (cit. on p. 1).
- [19] R. Mukherjee et al. “Many-body physics with alkaline-earth Rydberg lattices”. In: *Journal of Physics B: Atomic, Molecular and Optical Physics* 44.18 (2011), p. 184010. ISSN: 0953-4075. DOI: [10.1088/0953-4075/44/18/184010](https://doi.org/10.1088/0953-4075/44/18/184010) (cit. on p. 1).
- [20] Masao Takamoto and Hidetoshi Katori. “Spectroscopy of the S01–P03 Clock Transition of Sr87 in an Optical Lattice”. In: *Physical Review Letters* 91.22 (2003). ISSN: 0031-9007. DOI: [10.1103/PhysRevLett.91.223001](https://doi.org/10.1103/PhysRevLett.91.223001) (cit. on p. 1).
- [21] Tetsuya Ido and Hidetoshi Katori. “Recoil-free spectroscopy of neutral Sr atoms in the Lamb-Dicke regime”. In: *Physical Review Letters* 91.5 (2003), p. 053001. ISSN: 0031-9007. DOI: [10.1103/PhysRevLett.91.053001](https://doi.org/10.1103/PhysRevLett.91.053001) (cit. on p. 1).
- [22] S. Mauger, J. Millen, and M. P. A. Jones. “Spectroscopy of strontium Rydberg states using electromagnetically induced transparency”. In: *Journal of Physics B: Atomic, Molecular and Optical Physics* 40.22 (2007), F319–F325. ISSN: 0953-4075. DOI: [10.1088/0953-4075/40/22/F03](https://doi.org/10.1088/0953-4075/40/22/F03). URL: <http://arxiv.org/pdf/0710.1245v2> (cit. on p. 1).
- [23] Thomas K. Langin, Grant M. Gorman, and Thomas C. Killian. “Laser cooling of ions in a neutral plasma”. In: *Science (New York, N.Y.)* 363.6422 (2019), pp. 61–64. DOI: [10.1126/science.aat3158](https://doi.org/10.1126/science.aat3158) (cit. on p. 1).
- [24] Alexandre Cooper et al. “Alkaline earth atoms in optical tweezers”. In: *Physical Review X* 8.4 (2018). DOI: [10.1103/PhysRevX.8.041055](https://doi.org/10.1103/PhysRevX.8.041055). URL: <http://arxiv.org/pdf/1810.06537v1> (cit. on p. 1).
- [25] A. Signoles et al. “Coherent Transfer between Low-Angular-Momentum and Circular Rydberg States”. In: *Physical Review Letters* 118.25 (2017), p. 253603. ISSN: 0031-9007. DOI: [10.1103/PhysRevLett.118.253603](https://doi.org/10.1103/PhysRevLett.118.253603) (cit. on p. 2).
- [26] D. A. Anderson et al. “Production and trapping of cold circular Rydberg atoms”. In: *Physical Review A* 88.3 (2013). ISSN: 1050-2947. DOI: [10.1103/PhysRevA.88.031401](https://doi.org/10.1103/PhysRevA.88.031401) (cit. on p. 2).
- [27] Sebastian Weber et al. “Calculation of Rydberg interaction potentials”. In: *Journal of Physics B: Atomic, Molecular and Optical Physics* 50.13 (2017), p. 133001. ISSN: 0953-4075. DOI: [10.1088/1361-6455/aa743a](https://doi.org/10.1088/1361-6455/aa743a) (cit. on pp. 2, 37, 40, 41).
- [28] N. Šibalić et al. “ARC: An open-source library for calculating properties of alkali Rydberg atoms”. In: *Computer Physics Communications* 220 (2017), pp. 319–331. ISSN: 00104655. DOI: [10.1016/j.cpc.2017.06.015](https://doi.org/10.1016/j.cpc.2017.06.015) (cit. on pp. 2, 26, 27, 33, 34, 41, 49).
- [29] Thomas F. Gallagher. *Rydberg Atoms*. Vol. no. 3. Cambridge Monographs on Atomic, Molecular and Chemical Physics. Cambridge: Cambridge University Press, 1994. ISBN: 978-0-521-38531-2 (cit. on pp. 3, 22, 35).

- [30] Christian Hölzl. “Towards High  $n$  Circular Rydberg States in Ultracold Atomic Gases”. Master’s Thesis. Stuttgart: University of Stuttgart, 10/22/2019. URL: <https://www.pi5.uni-stuttgart.de/documents/abgeschlossene-arbeiten/2019-Hoelzl-Christian-Towards-High-n-Circular-Rydberg-States-in-Ultracold-Atomic-Gases-MSc.pdf> (cit. on p. 4).
- [31] C. J. Foot. *Atomic physics*. Oxford master series in atomic, optical and laser physics. Oxford: Oxford University Press, 2005. ISBN: 0198506953 (cit. on pp. 5, 7, 9).
- [32] Brian Harold Bransden and Charles Jean Joachain. *Physics of atoms and molecules*. 2nd ed., [reprint.] Harlow: Prentice Hall, 2003. ISBN: 0-582-35692-X (cit. on pp. 5, 11).
- [33] Charlotte Froese Fischer. “The solution of Schrödinger’s equation for two-electron systems by an MCHF procedure”. In: *Journal of Computational Physics* 13.4 (1973), pp. 502–521. ISSN: 00219991. DOI: [10.1016/0021-9991\(73\)90030-2](https://doi.org/10.1016/0021-9991(73)90030-2) (cit. on p. 6).
- [34] Vaeck, Godefroid, and Hansen. “Multiconfiguration Hartree-Fock calculations for singlet terms in neutral strontium”. In: *Physical review. A, General physics* 38.6 (1988), pp. 2830–2845. ISSN: 0556-2791. DOI: [10.1103/PhysRevA.38.2830](https://doi.org/10.1103/PhysRevA.38.2830) (cit. on p. 6).
- [35] B. V. Noumerov. “A Method of Extrapolation of Perturbations”. In: *Monthly Notices of the Royal Astronomical Society* 84.8 (1924), pp. 592–602. ISSN: 0035-8711. DOI: [10.1093/mnras/84.8.592](https://doi.org/10.1093/mnras/84.8.592) (cit. on p. 6).
- [36] Torsten Fließbach. *Lehrbuch zur theoretischen Physik*. 5. Aufl. Heidelberg: Spektrum Akademischer Verlag, 2007-2012. ISBN: 3-8274-2021-0 (cit. on p. 7).
- [37] Eugen Wigner. *Gruppentheorie und ihre Anwendung auf die Quantenmechanik der Atomspektren*. Wiesbaden: Vieweg+Teubner Verlag, 1931. ISBN: 978-3-663-00642-8. DOI: [10.1007/978-3-663-02555-9](https://doi.org/10.1007/978-3-663-02555-9) (cit. on p. 8).
- [38] Ingolf V. Hertel and Claus-Peter Schulz. *Atoms, molecules and optical physics*. Berlin: Springer, 2015. ISBN: 978-3-642-54321-0 (cit. on pp. 8, 9).
- [39] Wolfgang Demtröder. *Experimentalphysik 3*. Springer Berlin Heidelberg, 2005. ISBN: 3-540-21473-9 (cit. on p. 8).
- [40] Marinescu, Sadeghpour, and Dalgarno. “Dispersion coefficients for alkali-metal dimers”. In: *Physical Review A* 49.2 (1994), pp. 982–988. ISSN: 1050-2947. DOI: [10.1103/PhysRevA.49.982](https://doi.org/10.1103/PhysRevA.49.982) (cit. on pp. 9, 30).
- [41] Rick Mukherjee. “Strong interactions in alkaline-earth Rydberg ensembles”. Dresden, Technische Universität Dresden, Diss., 2014. Dresden: Sächsische Landesbibliothek-Staats- und Universitätsbibliothek Dresden and Technische Universität Dresden, 2014 (cit. on pp. 10, 11).
- [42] P. Fuentealba et al. “Pseudopotential calculations for alkaline-earth atoms”. In: *Journal of Physics B: Atomic and Molecular Physics* 18.7 (1985), pp. 1287–1296. ISSN: 0022-3700. DOI: [10.1088/0022-3700/18/7/010](https://doi.org/10.1088/0022-3700/18/7/010) (cit. on pp. 10, 12).
- [43] Patricio Fuentealba et al. “A proper account of core-polarization with pseudopotentials: single valence-electron alkali compounds”. In: *Chemical Physics Letters* 89.5 (1982), pp. 418–422. ISSN: 00092614. DOI: [10.1016/0009-2614\(82\)80012-2](https://doi.org/10.1016/0009-2614(82)80012-2) (cit. on p. 10).
- [44] Charles E. Burkhardt and Jacob J. Leventhal. *Topics in Atomic Physics*. [New York]: Springer Science+Business Media, Inc, 2006. ISBN: 978-0-387-31074-9 (cit. on p. 13).
- [45] Drake and Swainson. “Quantum defects and the  $1/n$  dependence of Rydberg energies: Second-order polarization effects”. In: *Physical Review A* 44.9 (1991), pp. 5448–5459. ISSN: 1050-2947. DOI: [10.1103/PhysRevA.44.5448](https://doi.org/10.1103/PhysRevA.44.5448) (cit. on p. 14).

- [46] Markus Mack et al. “Measurement of absolute transition frequencies of Rb87 to nS and nD Rydberg states by means of electromagnetically induced transparency”. In: *Physical Review A* 83.5 (2011). ISSN: 1050-2947. DOI: [10.1103/PhysRevA.83.052515](https://doi.org/10.1103/PhysRevA.83.052515) (cit. on p. 15).
- [47] C. L. Vaillant, M. P. A. Jones, and R. M. Potvliege. “Long-range Rydberg–Rydberg interactions in calcium, strontium and ytterbium”. In: *Journal of Physics B: Atomic, Molecular and Optical Physics* 45.13 (2012), p. 135004. ISSN: 0953-4075. DOI: [10.1088/0953-4075/45/13/135004](https://doi.org/10.1088/0953-4075/45/13/135004) (cit. on pp. 17, 19).
- [48] Christophe Louis J. Vaillant. “Long-Range Interactions in One- and Two-Electron Rydberg Atoms”. Dissertation. Durham: University of Durham, 2014. URL: <http://etheses.dur.ac.uk/10594/> (cit. on pp. 19–21).
- [49] M. S. Safronova and U. I. Safronova. “Critically evaluated theoretical energies, lifetimes, hyperfine constants, and multipole polarizabilities in Rb87”. In: *Physical Review A* 83.5 (2011). ISSN: 1050-2947. DOI: [10.1103/PhysRevA.83.052508](https://doi.org/10.1103/PhysRevA.83.052508). URL: <https://link.aps.org/doi/10.1103/PhysRevA.83.052508> (cit. on p. 20).
- [50] M. J. Seaton. “Coulomb functions for attractive and repulsive potentials and for positive and negative energies”. In: *Computer Physics Communications* 146.2 (2002), pp. 225–249. ISSN: 00104655. DOI: [10.1016/S0010-4655\(02\)00275-8](https://doi.org/10.1016/S0010-4655(02)00275-8) (cit. on p. 20).
- [51] J. R. Rubbmark and S. A. Borgström. “Rydberg Series in Strontium Found in Absorption by Selectively Laser-Excited Atoms”. In: *Physica Scripta* 18.4 (1978), pp. 196–208. ISSN: 0031-8949. DOI: [10.1088/0031-8949/18/4/002](https://doi.org/10.1088/0031-8949/18/4/002) (cit. on pp. 22, 51).
- [52] J. E. Sansonetti and G. Nave. “Wavelengths, Transition Probabilities, and Energy Levels for the Spectrum of Neutral Strontium (SrI)”. In: *Journal of Physical and Chemical Reference Data* 39.3 (2010), p. 033103. ISSN: 0047-2689. DOI: [10.1063/1.3449176](https://doi.org/10.1063/1.3449176) (cit. on pp. 22, 27).
- [53] Rudolph E. Langer. “On the Connection Formulas and the Solutions of the Wave Equation”. In: *Physical Review* 51.8 (1937), pp. 669–676. ISSN: 0031-899X. DOI: [10.1103/PhysRev.51.669](https://doi.org/10.1103/PhysRev.51.669) (cit. on p. 23).
- [54] Robert Löw et al. “An experimental and theoretical guide to strongly interacting Rydberg gases”. In: *Journal of Physics B: Atomic, Molecular and Optical Physics* 45.11 (2012), p. 113001. ISSN: 0953-4075. DOI: [10.1088/0953-4075/45/11/113001](https://doi.org/10.1088/0953-4075/45/11/113001). URL: <http://arxiv.org/pdf/1202.2871v1> (cit. on p. 32).
- [55] J. Millen et al. “Spectroscopy of a cold strontium Rydberg gas”. In: *Journal of Physics B: Atomic, Molecular and Optical Physics* 44.18 (2011), p. 184001. ISSN: 0953-4075. DOI: [10.1088/0953-4075/44/18/184001](https://doi.org/10.1088/0953-4075/44/18/184001) (cit. on p. 49).
- [56] D. Delande and J. C. Gay. “A New Method for Producing Circular Rydberg States”. In: *Europhysics Letters (EPL)* 5.4 (1988), pp. 303–308. ISSN: 0295-5075. DOI: [10.1209/0295-5075/5/4/004](https://doi.org/10.1209/0295-5075/5/4/004) (cit. on p. 50).
- [57] R. Beigang et al. “Determination of absolute level energies of 5sns1S0 and 5snd1D2 Rydberg series of Sr”. In: *Optics Communications* 42.1 (1982), pp. 19–24. ISSN: 00304018. DOI: [10.1016/0030-4018\(82\)90082-7](https://doi.org/10.1016/0030-4018(82)90082-7) (cit. on p. 51).
- [58] R. Beigang et al. “One-Photon Laser Spectroscopy of Rydberg Series from Metastable Levels in Calcium and Strontium”. In: *Physica Scripta* 26.3 (1982), pp. 183–188. ISSN: 0031-8949. DOI: [10.1088/0031-8949/26/3/007](https://doi.org/10.1088/0031-8949/26/3/007) (cit. on p. 51).
- [59] J. A. Armstrong, J. J. Wynne, and P. Esherick. “Bound, odd-parity J = 1 spectra of the alkaline earths: Ca, Sr, and Ba”. In: *Journal of the Optical Society of America* 69.2 (1979), p. 211. ISSN: 0030-3941. DOI: [10.1364/JOSA.69.000211](https://doi.org/10.1364/JOSA.69.000211) (cit. on p. 51).

- [60] Peter Esherick. “Bound, even-parity  $J=0$  and  $J=2$  spectra of Sr”. In: *Physical Review A* 15.5 (1977), pp. 1920–1936. ISSN: 1050-2947. DOI: [10.1103/PhysRevA.15.1920](https://doi.org/10.1103/PhysRevA.15.1920) (cit. on p. 51).

## Danksagung

An dieser Stelle möchte ich mich gerne bei einigen Personen bedanken, welche mir während meiner Bachelorarbeit, und auch außerhalb, stets zu Seite standen.

Zunächst danke ich **Prof. Dr. Tilman Pfau** für die Möglichkeit, meine Bachelorarbeit am 5. Physikalischen Institut absolvieren zu können. Diese Möglichkeit eröffnete mir viele Erkenntnisse in Bezug auf wissenschaftliche Arbeit und Forschung im Allgemeinen.

Weiterhin möchte ich mich bei **Dr. Florian Meinert** für seine sehr hilfreichen Beiträge in Bezug auf den theoretischen Hintergrund meiner Arbeit bedanken. Seine Erklärungen brachten immer einen neuen Blickwinkel auf das Problem hervor.

Ein besonderer Dank gilt **Christian Hölzl** für die Betreuung meiner Arbeit und die Hilfe bei allen Problemen, ob physikalischer oder numerischer Natur. Seine Betreuung half stets, die Arbeit mit guter Laune zu bewältigen.

Im Zuge dessen gilt auch dem Rest der **Circular Rydberg States Arbeitsgruppe** und natürlich der **Superatoms Arbeitsgruppe** ein Dankeschön für die nette Arbeitsatmosphäre und die Hilfe im Bezug auf die Arbeit.

Auch dem Sekretariat des Intituts und besonders **Anne-Katrin Kriesch** sei gedankt für die organisatorische Unterstützung.

Mein letzter Dank gilt meinen **Freunden** und insbesondere meiner **Familie**, welche mich stets in meinem Traum, Physik zu studieren, unterstützten. Dafür bin ich euch sehr dankbar.